

1 **Characterizing Changes in Eastern U.S. Pollution Events in a Warming World**

2 **A. M. Fiore^{1,2,*}, G.P. Milly², Laurel Quiñones^{3†}, Jared Bowden⁴, Sarah E. Hancock⁵, Erik**
3 **Helstrom^{2,‡}, Jean-François Lamarque⁶, Jordan Schnell^{7&}, Jason West⁸, and Yangyang Xu⁹**

4 ¹Department of Earth and Environmental Science, Columbia University, Palisades, NY, USA,

5 ²Lamont-Doherty Earth Observatory, Columbia University, Palisades, NY, USA, ³Department of
6 Applied Physics and Applied Mathematics, Columbia University, New York, NY, USA,

7 ⁴Department of Applied Ecology, North Carolina State University, Raleigh, NC, USA,

8 ⁵Department of Computer Science, Columbia University, New York, NY, USA, ⁶Climate and
9 Global Dynamics Laboratory, National Center for Atmospheric Research, Boulder, CO, USA,

10 ⁷Department of Earth and Planetary Sciences and Institute for Sustainability and Energy at

11 Northwestern University, Evanston, Illinois, USA, ⁸Department of Environmental Sciences &

12 Engineering, University of North Carolina, Chapel Hill, NC, USA, ⁹Department of Atmospheric

13 Sciences, Texas A&M University, College Station, TX, USA

14 Corresponding author: Arlene M. Fiore (amfiore@ldeo.columbia.edu)

15 *now at Department of Earth, Atmospheric, and Planetary Sciences, Massachusetts Institute of
16 Technology, Cambridge, MA, USA

17 †now at Department of Mechanical Engineering, Columbia University, New York, NY, USA

18 ‡now at Department of Civil and Environmental Engineering, Massachusetts Institute of
19 Technology, Cambridge, MA, USA

20 &now at Cooperative Institute for Research in Environmental Sciences, University of Colorado
21 Boulder; NOAA Global Systems Laboratory, Boulder, CO, USA

22 **Key Points:**

- 23 • Frequency and duration of Northeast US pollution events increase along with heat events
24 under a high-warming scenario.
- 25 • EOF approach enables rapid assessment of regional-scale changes in pollution events
26 without needing to bias correct models individually.
- 27 • Larger uncertainty in EUS PM_{2.5} from different model responses to climate change than
28 from climate variability.

29

30 **Abstract**

31 Risk assessments of air pollution impacts on human health and ecosystems would ideally
32 consider a broad set of climate and emission scenarios and the role of natural internal climate
33 variability within a single scenario. We analyze initial condition chemistry-climate ensembles to
34 gauge the significance of greenhouse-gas-induced air pollution changes relative to internal
35 climate variability, and response differences in two models. To quantify the effects of climate
36 change on the frequency and duration of summertime regional-scale pollution episodes over the
37 Eastern United States (EUS), we apply an Empirical Orthogonal Function (EOF) analysis to a 3-
38 member GFDL-CM3 ensemble with prognostic ozone and aerosols and a 12-member NCAR-
39 CESM1 ensemble with prognostic aerosols under a 21st century RCP8.5 scenario with air
40 pollutant emissions frozen in 2005. Correlations between GFDL-CM3 principal components for
41 ozone, PM_{2.5} and temperature represent spatiotemporal relationships discerned previously from
42 observational analysis. Over the Northeast region, both models simulate summertime surface
43 temperature increases of over 5 °C from 2006-2025 to 2081-2100 and PM_{2.5} of up to 1-4 μg m⁻³.
44 The ensemble average decadal incidence of upper quartile Northeast PM_{2.5} events lasting at least
45 five days doubles in GFDL-CM3 and increases >50% in NCAR-CESM1. In other EUS regions,
46 inter-model differences in PM_{2.5} responses to climate change cannot be explained by internal
47 climate variability. Our EOF-based approach anticipates future opportunities to data-mine initial
48 condition chemistry-climate model ensembles for probabilistic assessments of changing
49 frequency and duration of regional-scale pollution and heat events while obviating the need to
50 bias-correct concentration-based thresholds separately in individual models.

51 **Plain Language Summary**

52 Prior studies conclude climate change will worsen air quality in some polluted regions but
53 typically neglected the role of climate variability. Uncertainty also arises from differences in
54 climate model responses to a given anthropogenic forcing scenario. Differentiating the relative
55 contributions of these uncertainties (structural versus stochastic) to inter-model differences in
56 projected air pollution responses to climate change is becoming possible with initial-condition
57 climate model ensembles. We analyze day-by-day variations in pollutant levels over five eastern
58 U.S. region to quantify changes in frequency and duration of regional-scale high pollution and
59 heat events with small initial-condition ensembles from two different models. Under a 21st
60 century climate change scenario in which air pollutant emissions are fixed at 2005 levels, our
61 analysis shows longer-lasting and more frequent Northeast U.S. PM_{2.5} (and heat) episodes, which
62 could exacerbate public health burdens. Projecting changes in other EUS regions is limited by
63 inter-model differences that exceed the uncertainty attributable to climate variability. While our
64 ensembles are small relative to those generated most recently with physical climate models, our
65 findings add to a growing recognition that climate variability complicates the detection and
66 attribution of observed and simulated air pollution trends under climate change scenarios.

67 **1 Introduction**

68 High ground-level concentrations of the top two U.S. air pollutants, fine particles (PM_{2.5}) and
69 ozone (O₃) sometimes co-occur along with high temperatures across the eastern U.S.A. (EUS)
70 during summer, with >50% same-day coincidence of at least two of these extremes in the Northeast
71 (Schnell & Prather, 2017) and generally about one-third coincidence in the highest O₃ and
72 temperature events (Phalitnonkiat et al., 2018). Air pollution health burdens in other mid-latitude
73 regions have also been found to increase during heat waves (Filleul et al., 2006; García-Herrera et

74 al., 2010; Shaposhnikov et al., 2014), although it is unknown if prolonged versus intermittent
75 exposure to high pollution events elicit different human health responses. Future increases in
76 intensity and frequency of heat stress events are expected (Coffel et al., 2017), raising the
77 possibility that climate change will also exacerbate air pollution and associated adverse health
78 outcomes. Here, we describe an approach to characterize changes in frequency and duration of
79 high pollution and heat events in simulations of 21st century climate change, with a primary focus
80 on PM_{2.5}, available from two models, and a secondary focus on the co-occurrence of high PM_{2.5},
81 O₃, and temperature events.

82 Prior studies identified changes in the severity, duration and spatial extent of U.S. air pollution
83 events under future climate scenarios (Mickley et al., 2004; Rieder et al., 2015; Schnell et al., 2016;
84 S. Wu et al., 2008). Compound extreme weather events such as simultaneous occurrence of air
85 stagnation and heat waves, which are likely to affect air pollution, are projected to increase by
86 mid-to-late century (J. Zhang et al., 2018). Xu et al. (2020) showed a ten-fold increase in the co-
87 occurrence of heatwaves and high PM_{2.5} events by mid-21st century. Air pollution has long been
88 observed to co-vary with meteorology on hourly to interannual time scales (*e.g.* Camalier et al.,
89 2007; Dawson et al., 2013; Kerr et al., 2019; Leibensperger et al., 2008; Lin et al., 2001; Logan,
90 1989; Rao et al., 1995; Tai et al., 2010; Vukovich, 1995), with an emphasis on air stagnation,
91 temperature inversions, heat waves, and wildfires responding to heat and drought as drivers of the
92 most extreme pollution events (Hong et al., 2019; Horton et al., 2012; Horton et al., 2014; Hou &
93 Wu, 2016; Konovalov et al., 2011; Porter & Heald, 2019; Porter et al., 2015; Shen et al., 2016;
94 Spracklen et al., 2009; Sun et al., 2017; Wang & Angell, 1999). Other work indicates that local
95 observed meteorology-pollutant relationships are strongly shaped by the underlying atmospheric
96 dynamics that control synoptic transport (Barnes & Fiore, 2013; Kerr et al., 2020; Kerr et al., 2019;
97 Oswald et al., 2015; Previdi & Fiore, 2019; Sun et al., 2019; Tai et al., 2012). Overall, a wide range
98 of modeling systems project that climate change will degrade air quality in some currently polluted
99 U.S. regions, although models disagree as to the regional extent and magnitude of projected air
100 pollution changes (*e.g.*, Fiore et al., 2015; Fu & Tian, 2019; Jacob & Winner, 2009; Kirtman et al.,
101 2013; Nolte et al., 2018; Schnell et al., 2016; Weaver et al., 2009).

102 Some of the inter-model disagreement in the published literature likely reflects a lack of
103 separation of forced climate change (*i.e.*, “signal” due to rising greenhouse gases plus aerosols)
104 from internal variability (*i.e.*, climate “noise” due to natural processes within the climate system)
105 (Deser et al., 2020; East & Garcia-Menendez, 2020; Garcia-Menendez et al., 2017). Computational
106 limitations restricted the length and number of simulations for most prior model projections of
107 future changes in air pollution (Fiore et al., 2015; Fiore et al., 2012; Jacob & Winner, 2009; Weaver
108 et al., 2009). Prior analysis of initial condition ensembles within a single climate model has
109 demonstrated a major role for internal climate variability, measured by the inter-ensemble range,
110 in shaping the near-term regional meteorological trends (Deser et al., 2012ab) to which air
111 pollution will respond. Each ensemble member is one possible future air pollution response to the
112 same forcing scenario, such that with sufficiently large ensembles, statistics can be developed to
113 quantify the probability of ‘rare’ events in the observed record. Extracting signals of climate
114 change is particularly challenging for extreme quantities. Advances in computational power now
115 permit large ensemble simulations with physical climate models (Deser et al., 2012ab; Deser et
116 al., 2013; Kay et al., 2015), where each ensemble member has different initial conditions but
117 otherwise is forced by the same greenhouse gas and aerosol emission scenarios. The range across
118 individual ensemble members offers a measure of the noise associated with internal climate
119 variability, while the ensemble mean provides an estimate of the forced signal.

120 Schnell et al. (2014; 2015) have previously concluded that coarse resolution global models
121 capture the observed spatial extent and timing of large-scale O₃ episodes, providing a strong basis
122 for our analysis of air pollution simulated by global climate models. Challenges to quantifying
123 simulated changes in high pollution events include selecting an appropriate threshold and
124 accounting for model biases that may require adjusting the model threshold to ensure a similar
125 frequency of high events as observed. Separate adjustments may be needed not only within each
126 individual model (e.g., as in Horton et al. (2012), but also each region of interest (Schnell et al.,
127 2015; Turnock et al., 2020).

128 Here, we examine changes in the frequency and duration of high pollution events over five
129 distinct EUS regions. We expand upon Eder et al. (1993), who first applied Empirical Orthogonal
130 Function (EOF) analysis to identify EUS regions in which ground-level ozone is high or low
131 simultaneously across the region. This statistical approach avoids the pervasive problem of
132 identifying relevant model thresholds in the presence of model biases by instead targeting model
133 skill at representing the underlying patterns of spatiotemporal variability. We probe the role of
134 natural climate variability, which arises internally within the climate system, as represented by two
135 chemistry-climate models with interactive aerosol simulations. We also consider co-variations in
136 high PM_{2.5}, O₃, and temperature events in one model with full tropospheric chemistry, and compare
137 to observed relationships. The approach described below can be applied to rapidly gauge changing
138 air pollution events as simulated by future large initial condition climate model ensembles that
139 include full tropospheric (gas-phase plus aerosol) chemistry.

140 **2 Data and Methods**

141 **2.1 Models and Observations**

142 Our analysis centers on an existing 3-member ensemble generated with the GFDL-CM3
143 chemistry-climate model to project air pollution during the 21st century under a high warming
144 scenario. We refer to this scenario as “RCP8.5_WMGG” in which Well-Mixed Greenhouse Gases
145 (WMGG) follow the RCP8.5 scenario. Both particulate matter (PM) and ozone precursor
146 emissions are held fixed at 2005 levels as described by Clifton et al. (2014). The simulated
147 warming is less than in the standard RCP8.5 scenario in which aerosol and precursor emissions
148 decline. The GFDL-CM3 model includes fully coupled ocean-atmosphere-sea ice-dynamic
149 vegetation land models, and stratospheric and tropospheric gas-phase chemistry and aerosols
150 (Austin et al., 2013; Donner et al., 2011; Naik et al., 2013). The native model resolution is a c48
151 cubed sphere which is post-processed to a 2°x2° horizontal grid. All RCP8.5_WMGG ensemble
152 members are identical except for their initial conditions, which are taken from the final day of a
153 corresponding transient 1860-2005 historical simulation. Each historical ensemble member was
154 launched using initial conditions sampled at 50-year intervals in a “pre-industrial control”
155 simulation that perpetually repeats 1860 greenhouse gas, aerosol, air pollutant emissions and other
156 forcings. RCP8.5_WMGG simulations use the same monthly-varying dry deposition and isoprene,
157 soil NO_x and biomass burning emissions every year. Diurnal cycles are imposed for isoprene
158 emissions and ozone dry deposition. Wet deposition and sources of lightning NO_x, dimethyl sulfide
159 (DMS), marine organic aerosol, sea salt and dust are coupled to the simulated meteorology and
160 thus respond to changes in climate (Naik et al., 2013). The simulations neglect feedbacks to air
161 pollution through wildland fires (Abatzoglou & Williams, 2016; Spracklen et al., 2009) as well as
162 changes in terrestrial biogenic emissions or dry deposition (Andersson & Engardt, 2010). These

163 idealized simulations enable us to isolate the influence of rising well-mixed greenhouse gases on
164 pollution events, mainly by changing the meteorology.

165 Hourly surface ozone, daily maximum temperature at 2m reference height (T_{\max}), daily
166 surface $PM_{2.5}$, and monthly chemical components of $PM_{2.5}$ were archived from the lowermost
167 atmospheric layer of all GFDL-CM3 simulations. The $PM_{2.5}$ diagnostic includes sulfate (assumed
168 to be ammonium sulfate), carbonaceous aerosol (organic matter, black carbon, and secondary
169 organic aerosol), the smallest size bin (of five) for dust, and the smallest two size bins (of five) for
170 sea salt. We calculate maximum daily 8-hour average (MDA8) ozone from the hourly ozone fields.

171 We draw on a 12-member ensemble with the CESM1 climate model generated at NCAR
172 to provide additional context for the changes in high- $PM_{2.5}$ and temperature events diagnosed with
173 the GFDL-CM3 ensemble. As described by Xu and Lamarque (2018), this coupled atmosphere-
174 ocean-sea ice-land model at $1^\circ \times 1^\circ$ horizontal resolution includes an interactive aerosol scheme
175 with three internally mixed modes (Ghan et al., 2012; Liu et al., 2012). As for GFDL-CM3, the
176 NCAR-CESM1 simulations hold aerosol and precursor emissions fixed at 2005 levels, as well as
177 the oxidant fields used to drive secondary aerosol formation, but greenhouse gas concentrations
178 rise along the RCP8.5 scenario from 2006 to 2100. In contrast to GFDL-CM3, the CESM1
179 configuration does not include the fully interactive tropospheric chemistry needed to simulate
180 changes in oxidants. Each NCAR-CESM1 ensemble member is configured identically except for
181 a tiny perturbation ($O(10^{-14})$ K) imposed in the atmospheric temperature initial condition fields
182 (Kay et al., 2015; Xu & Lamarque, 2018). Dust and sea salt emissions respond to meteorology and
183 land surface conditions, while biogenic VOC emissions are held constant (Lamarque et al., 2011).
184 $PM_{2.5}$ is defined as the sum of daily mean sulfate, dust, black carbon, and primary and secondary
185 organic aerosol in the Aitken and accumulation mode in the lowermost atmospheric layer, which
186 we convert from the native model mass mixing ratio (kg/kg) to mass density ($\mu\text{g}/\text{m}^3$). We also use
187 daily mean temperatures at the surface and at 2m reference height from these simulations.

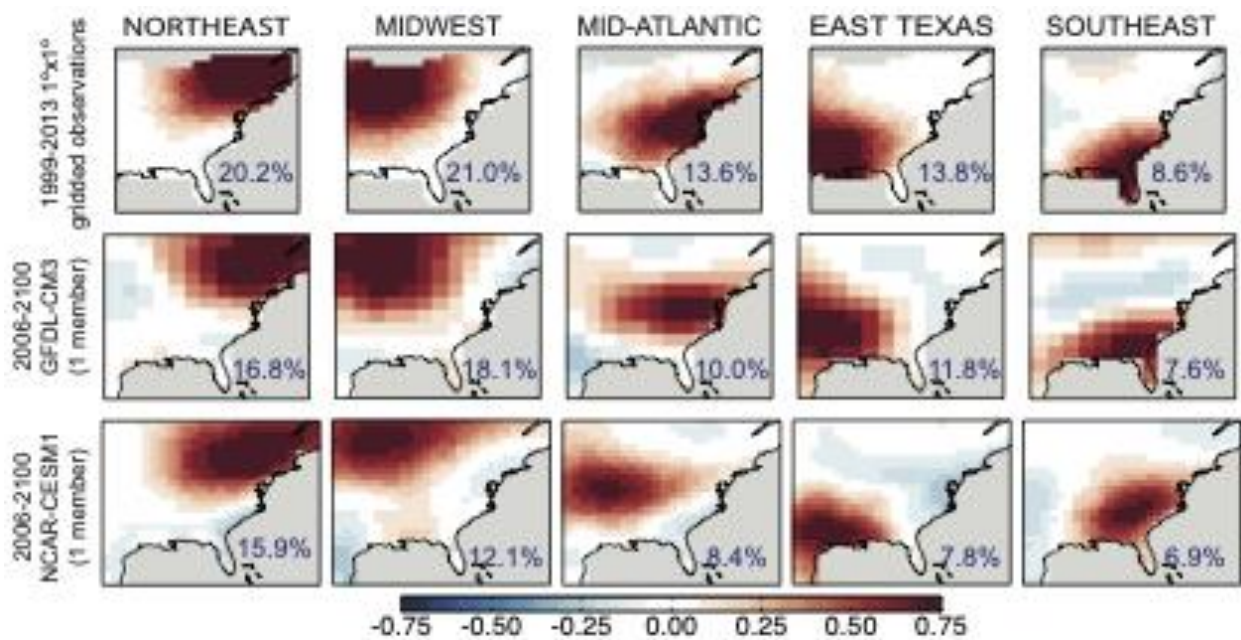
188 To evaluate simulated EUS spatiotemporal patterns in air pollution, we use observations
189 of near-surface daily mean $PM_{2.5}$ and MDA8 ozone measured at U.S. and Canadian ground-based
190 networks that were optimally interpolated to a $1^\circ \times 1^\circ$ grid over the EUS (Schnell et al., 2014;
191 Schnell & Prather, 2017). These gridded datasets are available for 1999-2013 and 1993-2013 for
192 $PM_{2.5}$ and ozone, respectively. We also use the $1^\circ \times 1^\circ$ temperature fields that Schnell and Prather
193 (2017) regridded from the $0.5^\circ \times 0.5^\circ$ European Centre for Medium-Range Weather Forecasting
194 (ECMWF) Interim reanalysis maximum daily 6-hourly temperatures sampled at 2 m reference
195 height.

196 2.2 Empirical Orthogonal Function (EOF) analysis

197 We analyze daily $PM_{2.5}$, ozone, and temperature data during summer (June-July-August).
198 We focus on summer, the season when ozone is highest, because we are interested in co-occurrence
199 of ozone and $PM_{2.5}$, which we examine in the GFDL-CM3 model (Section 5). Before conducting
200 Empirical Orthogonal Function (EOF) analysis, we standardize all data, separately for each grid
201 cell, by removing the mean of the entire time series and dividing by the standard deviation. The
202 EOFs are the eigenvectors of the covariance matrix derived from the data matrix (dimensioned
203 space by time). Each EOF is a spatial loading pattern for a mode of spatiotemporal variability that
204 identifies where air pollution or temperature varies coherently (*i.e.*, polluted/clean air and hot/cold

205 temperatures occur across the region indicated by the EOF at the same time). For some of the
 206 analysis below we use the EOFs to define a regional mask where the EOF loading exceeds 0.5.

207 The first five EOFs derived from the PM_{2.5} observations capture 77% of the variance in
 208 daily summertime PM_{2.5} concentrations over the EUS (Figure 1). The EOFs derived from the
 209 observed MDA8 O₃ and daily maximum temperature datasets capture 77% and 73% of the total
 210 variance, respectively. We select five EOFs for Varimax rotation after considering a change point
 211 for the amount of variance explained by each successive EOF derived from observations (Wilks,
 212 1995). Table S1 lists the variance explained by the first ten EOFs. We retain the first five EOFs
 213 across all variables. The EOF analysis thus reduces the dataset size for further temporal analysis,
 214 from the number of individual grid cells (424, 447, and 424 from the gridded PM_{2.5}, ozone, and
 215 temperature observations, respectively) to five EUS regions. Below we refer to the EOFs by the
 216 region names shown in Figure 1.



217

218 **Figure 1.** Regions emerging from an EOF analysis on standardized anomalies of summertime
 219 daily surface PM_{2.5} over the EUS. Shown are the EOF pattern loadings derived from (top)
 220 gridded observations, (middle) one of three ensemble members in the GFDL-CM3 chemistry-
 221 climate model, and (bottom) one of 12 NCAR-CESM1 ensemble members. Blue text indicates
 222 the total variance explained by each EOF.

223 Prior analysis of summertime daily ground-level ozone over the EUS for earlier time
 224 periods revealed similar EOFs to those in Figure 1 (Eder et al., 1993; Fiore et al., 2003; Lehman
 225 et al., 2004). The EOFs derived from summertime ground-level MDA8 ozone observations (Figure
 226 S1a) spatially correlate with those for PM_{2.5} ($r = 0.93-0.99$ highest in the Northeast). EOFs for
 227 daily T_{max} (Figure S1b) also correlate with those for PM_{2.5} ($r = 0.85-0.95$, highest in the Northeast
 228 and Upper Midwest).

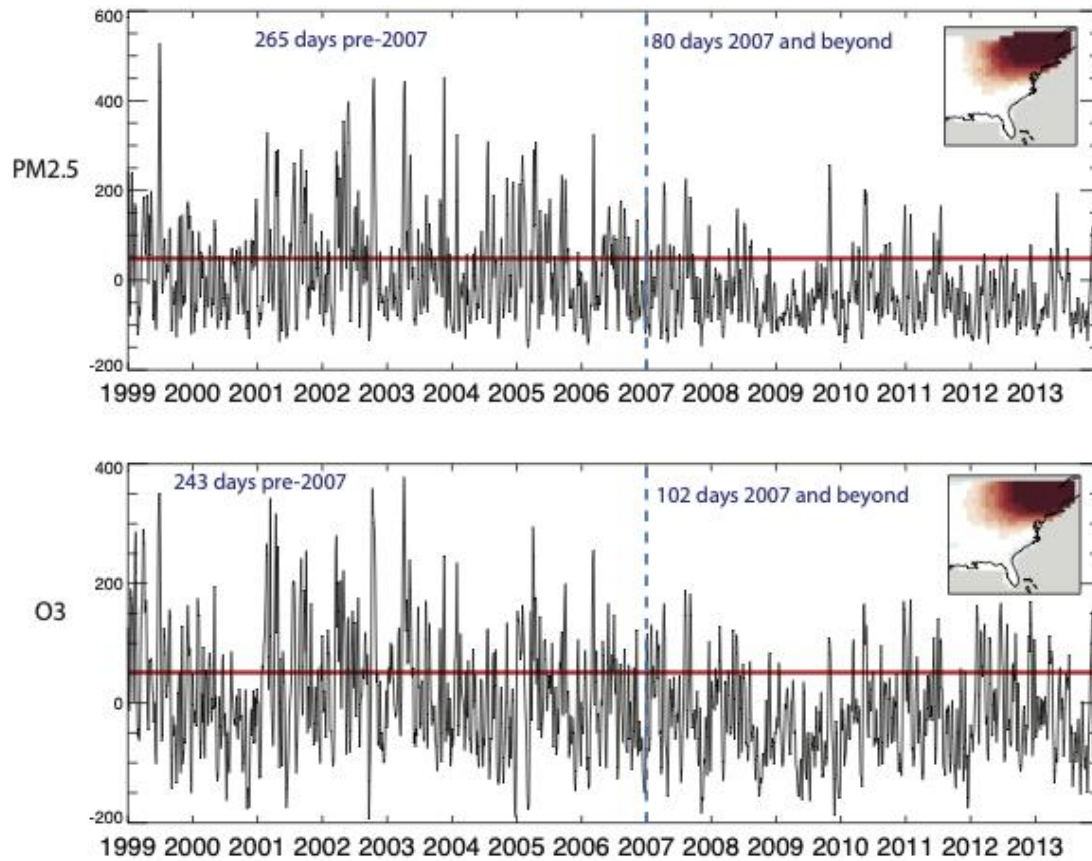
229 We apply a parallel analysis to the model data; see Tables S2-S3ab for variance explained
 230 by the first 10 raw EOFs in the GFDL-CM3 (PM_{2.5}, O₃ and temperature) and CESM1 (PM_{2.5} and

231 temperature only) models, respectively (Figures 1, S1ab). The spatial dimension decreases from
232 113 grid cells in the GFDL-CM3 model and 465 from CESM1 to five regions. We confirm in the
233 GFDL model that the EOFs change little under the 21st century climate change scenario, by
234 conducting the EOF analysis separately on the simulated daily PM_{2.5} for 2006-2025 versus 2086-
235 2100 (Figure S2). We also find that the EOFs are robust across ensemble members (Figures S3ab).

236 Each EOF is accompanied by a principal component (PC) time series spanning summer
237 days in all years. By definition, the PCs are uncorrelated and combine linearly to explain the
238 largest possible variance captured by the reduced version of the overall dataset. The PC represents
239 how strongly expressed a particular EOF is on each summer day. We orient each PC such that high
240 pollution or temperature values are positive. These time series are the foci for our analysis of
241 changes in the frequency and duration of regional-scale high-pollution events.

242 We illustrate how the PC can be used to quantify the number of summertime regional-scale
243 pollution events for the Northeast (Figure 2). We consider the observational period during which
244 numerous studies have documented decreasing EUS air pollution in response to emission control
245 programs implemented in the 1990s and 2000s (*e.g.*, Boys et al., 2014; Cooper et al., 2012; Frost
246 et al., 2006; Murphy et al., 2011). For example, 60% decreases in sulfur dioxide emissions from
247 1990 to 2010 have been linked to 45% lower sulfate aerosol (Skylakou et al., 2021). Summertime
248 ozone decreases have been attributed to NO_x and VOC emissions reductions of 40% and 14%,
249 respectively, from 2002-2011 (Simon et al., 2015). We define events in the upper quartile (75th
250 percentile; red line in Figure 2) as ‘high’. To quantify changes in observed high PM_{2.5} and O₃
251 events, we count the number of days on which the PC exceeds this threshold. From 1999-2006 to
252 2007-2013 (time periods separated by the blue dashed vertical line in Figure 2), the number of
253 observed days with high pollution over the Northeast drops: from 265 to 80 days for PM_{2.5} and
254 from 243 to 102 days for MDA8 O₃. This EOF analysis thus enables us to diagnose changes in the

255 frequency of regional-scale high pollution events, without defining an event locally at each
 256 monitor or model grid cell relative to a specific concentration threshold.



257

258 **Figure 2.** Proof-of-concept demonstration of EOF analysis to track high pollution events.
 259 Northeast principal components derived from observed summertime (top) daily mean PM_{2.5} and
 260 (bottom) MDA8 ozone from 1999-2013. Shown are the 75th percentile thresholds (red lines)
 261 used to define and count the number of high regional-scale pollution events.

262 Our analysis does not focus on the magnitude of the pollution levels during these events.
 263 Rather, our primary interest is to define changes in event frequency and duration, and co-
 264 occurrence of high PM_{2.5}, O₃, and temperature events under the RCP8.5_WMGG climate change
 265 scenario for the 21st century. In any case, the largest, longest-lasting pollution episodes –
 266 especially those that are coincident (*i.e.*, high heat, high O₃, and high PM_{2.5}) – typically have the
 267 highest pollution levels (Schnell and Prather, 2017).

268 3 Model Evaluation

269 Typical approaches evaluating models with observations at specific locations and times are
 270 problematic for our study. First, these free-running, fully-coupled chemistry-climate models
 271 generate their own weather and thus cannot reproduce the climate variability present in the real
 272 atmosphere that is stochastic but imprinted on the air pollutant measurements (*e.g.* year-to-year
 273 variations). These measurements are available for a limited number of years when considering
 274 variability but can be helpful for evaluating mean errors. Second, the simulations cannot capture

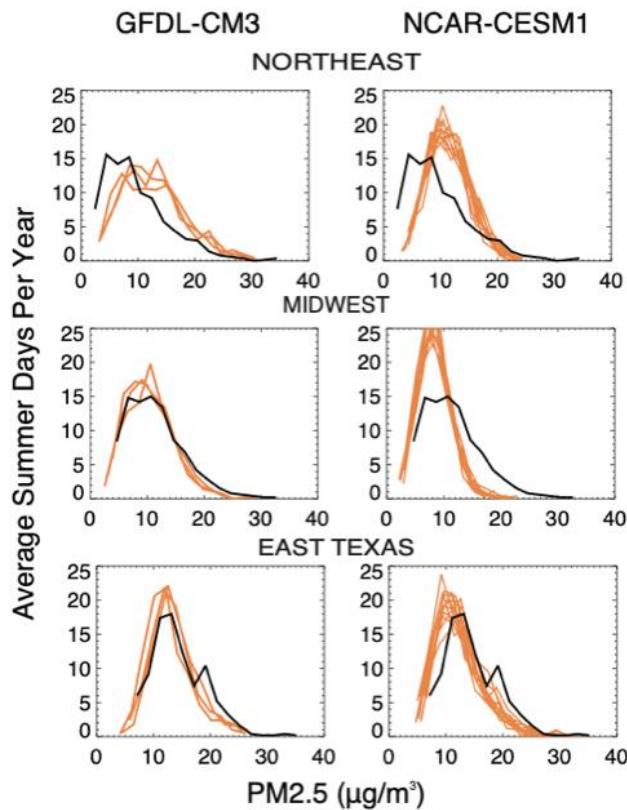
275 observed trends due to changing anthropogenic emissions (since 2005) because they hold air
276 pollutant emissions constant at 2005 levels. In light of these challenges, we evaluate three aspects
277 of the simulations: (1) simulated multi-year summertime average $PM_{2.5}$ and the dominant chemical
278 components (sulfate and organic carbon versus observations, (2) EOFs derived from modeled
279 versus observed daily $PM_{2.5}$, and (3) probability distributions of regionally averaged daily $PM_{2.5}$
280 derived from the same datasets as in (2). Application of the EOF analysis does not require exact
281 space-time matching, and is ideally suited to evaluate spatiotemporal patterns in climate models
282 that generate their own weather and thus cannot be expected to reproduce observations at a
283 particular location and time. This spatiotemporal evaluation, however, requires extensive
284 observational networks with data of sufficient length and quality, such as are available over the
285 EUS. Section 5 additionally compares observed and simulated cross-correlative relationships
286 between regions and variables.

287 *Summertime mean $PM_{2.5}$ and its major components.* The summertime ensemble mean $PM_{2.5}$
288 simulated by both models reflects the observed spatial pattern of summertime ensemble mean
289 $PM_{2.5}$ in the gridded observations. The NCAR-CESM1 simulation is biased high over the
290 Southeast (Figure S4a). Comparison with the IMPROVE network (Solomon et al., 2014) suggests
291 that both tend to models overestimate EUS $PM_{2.5}$ at these rural sites (Figure S4b), although we
292 note that the comparison with the gridded observations at spatial scales similar to the horizontal
293 resolution of the models is most pertinent here. We also evaluate chemical composition at the
294 IMPROVE sites, which reveals that CESM1 simulates excessive organic carbon, although sulfate
295 tends to be biased low. GFDL-CM3 has a slight tendency to overestimate both species at the
296 IMPROVE sites.

297 *EOFs derived from summertime daily $PM_{2.5}$.* The regional patterns that emerge from the EOF
298 analysis applied to daily surface $PM_{2.5}$ are similar in the observations from 1999-2013 and from
299 each of the three GFDL-CM3 model ensemble members for the 2006-2100 period (Figure 1 and
300 S3a). The CM3-derived EOFs capture less overall variance (64-65%; range is over ensemble
301 members) than the observation-derived EOFs (77%). The overall similarity of the patterns implies
302 that this model captures the underlying dynamical and chemical processes that shape the observed
303 spatiotemporal variability. Figure 1 also shows EOFs derived from summertime daily $PM_{2.5}$
304 simulated by one NCAR-CESM1 ensemble member (Figure S3b displays other ensemble
305 members). The $PM_{2.5}$ EOFs derived from CESM1 capture 54% of the overall variance in the
306 modeled dataset, and four of the EOFs correspond to those derived from observations (Figure 1).
307 Rather than a coastal mid-Atlantic EOF, CESM1 highlights a spatial mode of variability centered
308 over Missouri and Kansas. The spatial error in this pattern as compared to the observation-derived
309 EOF may reflect shortcomings in the geographical placement of the Atlantic or Pacific subtropical
310 high pressure systems and the Great Plains Low Level Jet, and their accompanying precipitation
311 patterns (Bowden et al., 2013; Li et al., 2013; Schmidt & Grise, 2019; Tang et al., 2017). The
312 Northeast EOF, where the two models agree most in their projected changes, serves as a major
313 focus of our analysis and is similarly well captured by both CESM1 and GFDL-CM3.

314 *Probability distributions of daily regional averaged $PM_{2.5}$ in summer.* From Figure 1, we
315 select grid cells in which the EOF loading exceeds 0.5 to define a regional mask separately for
316 each model and the observations. We apply this mask to calculate a daily regional mean $PM_{2.5}$ for
317 the 2006-2010 and 2003-2007 time periods for the models and observations, respectively, and sort
318 the data into $2 \mu\text{g m}^{-3}$ concentration bins. The mis-match of time periods reflects a compromise

319 to align the model, with constant year 2005 emissions, and the observations, with a 5-year period
 320 intended to minimize influences from both emission trends and weather fluctuations. Figure 3
 321 shows the distribution of the average number of days each summer as a function of regional mean
 322 $\text{PM}_{2.5}$ concentrations for the Northeast, Upper Midwest, and East Texas regions (Figure S5 shows
 323 the mid-Atlantic and Southeast). The individual GFDL-CM3 ensemble members fall near or span
 324 the observed frequency for the $\text{PM}_{2.5}$ bins $> 22 \mu\text{g m}^{-3}$ (Figure 3). This high tail is most relevant to
 325 understanding how high $\text{PM}_{2.5}$ events will change as the planet warms, and is generally better
 326 captured by GFDL-CM3 than CESM1, except over the East Texas region where GFDL-CM3
 327 captures the mode but underestimates the frequency of the highest $\text{PM}_{2.5}$ concentrations ($> 17 \mu\text{g m}^{-3}$;
 328 Figure 3). While the mode over East Texas is underestimated by CESM1, some ensemble
 329 members simulate observed $\text{PM}_{2.5}$ levels $> 26 \mu\text{g m}^{-3}$ as observed. The GFDL-CM3 distributions
 330 over the Northeast, mid-Atlantic and Southeast reflect the mean positive bias evident from Figures
 331 S4ab. In CESM1, the positive bias is even higher over the Northeast (and Southeast), with little
 332 similarity to the observed distribution shape. Despite mis-placing the Mid-Atlantic EOF relative
 333 to observations, CESM1 captures the mode with a slight underestimate, but misses the high tail of
 334 the distribution (Figure S5). Below we analyze more deeply high events in GFDL-CM3, which
 335 enables us to examine high events of surface O_3 alongside $\text{PM}_{2.5}$ and temperature. The NCAR-
 336 CESM1 simulations provide a broader context on inter-model differences and on climate
 337 variability as measured by the range across ensemble members.



338

339 **Figure 3.** Distributions of the number of summer days with regionally averaged daily $\text{PM}_{2.5}$
 340 falling within $2 \mu\text{g m}^{-3}$ concentration bins. Averages are taken over the regions where the EOF
 341 loading in Figure 1 exceeds > 0.5 in the observations (black) for the years 2003-2007 and in the

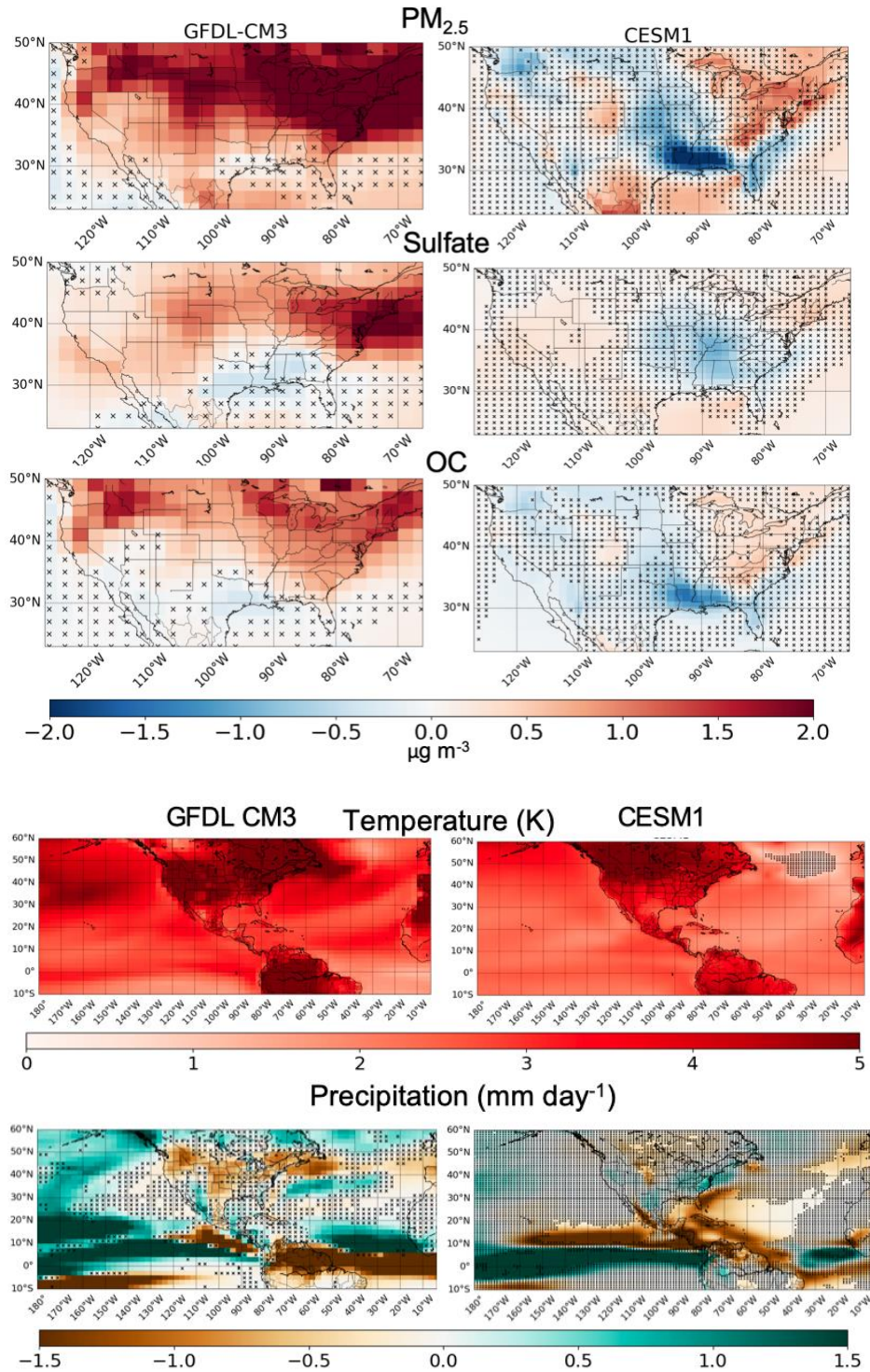
342 individual (orange) GFDL-CM3 (left) NCAR-CESM1 (right) ensemble members over the
343 Northeast (top), Midwest (middle), and East Texas (bottom) for model years 2006-2010.

344 **4 21st Century Changes in Summertime PM_{2.5}**

345 4.1 Mean values, composition, and probability density functions

346 Summertime mean PM_{2.5} increases across the contiguous U.S.A. during the 21st century in
347 the GFDL-CM3 ensemble mean, with the largest increases occurring over the Northeast and Upper
348 Midwest, by up to 1-2 and 3-4 $\mu\text{g m}^{-3}$ by mid- (2041-2060; Figure S6) and end-of-century (2081-
349 2100; Figure 4), respectively. These changes are deemed significant if the ensemble mean change
350 exceeds the inter-ensemble range of simulated changes. Grid cells labeled with an 'x' in Figures 4
351 and S6 do not meet this significance criterion. CESM1 projects smaller ensemble mean PM_{2.5}
352 increases ($<1.5 \mu\text{g m}^{-3}$) across the Northeast by end-of-century, and decreases over Louisiana,
353 southern Mississippi and Alabama of more than $0.5 \mu\text{g m}^{-3}$ and $2 \mu\text{g m}^{-3}$ by mid- and end-of-
354 century, respectively. By 2081-2100, CESM1 also simulates decreases exceeding $0.5 \mu\text{g m}^{-3}$ over
355 the central Plains, in some of the Northwest and along the southern Atlantic seaboard, though many
356 of these decreases are not significant (Figure 4). In both models, sulfate and organic carbon drive
357 PM_{2.5} increases in the Northeast, with organic carbon contributing more to simulated changes in

358 the Southeast. Significant sulfate increases are projected by both models in parts of the West.
 359 GFDL-CM3 also simulates organic carbon increases in the Northwest.



360

361

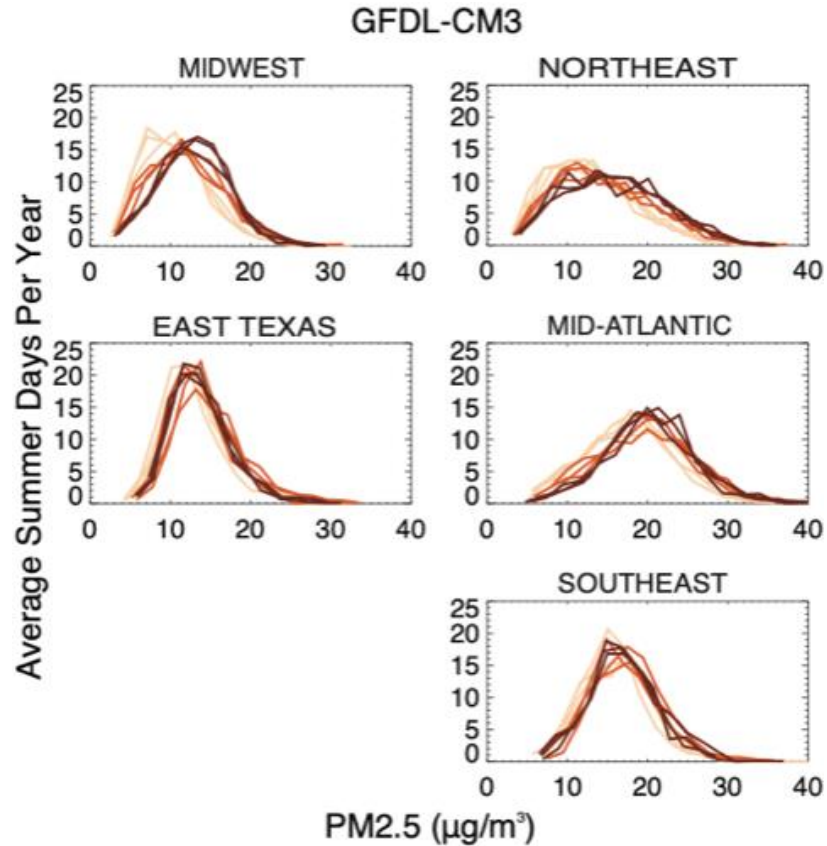
362 **Figure 4.** Change in summertime (June-July-August) PM_{2.5}, sulfate, organic carbon (OC), daily
 363 2m air temperature (max for GFDL-CM3; mean for CESM1), and precipitation from 2006-2025
 364 to 2081-2100, simulated with GFDL-CM3 (left; 3 ensemble member mean) and CESM1 (right; 12

365 ensemble member mean) for the RCP8.5_WMGG scenario. Grid cells marked with 'x' indicate
366 that the ensemble mean change is smaller than the range of the changes simulated by individual
367 ensemble members.

368 Simulated changes in average temperature and precipitation are also shown in Figures 4
369 and S6. Summertime daily maximum near-surface air temperatures warm in both models, by over
370 2 K and 4 K by mid- and end-of-century respectively. While GFDL-CM3 simulates a warmer,
371 drier summer over the Northeast, CESM1 warms but wettens (though insignificantly). We do not
372 find evidence that a warmer and drier climate always accompanies higher PM_{2.5}, or that more
373 rainfall lowers PM_{2.5}. For example, CESM1 simulates declining PM_{2.5} along the Gulf coast without
374 increasing precipitation, which instead increases northeast of this region. Earlier work also
375 demonstrated complex relationships between PM_{2.5} and meteorology that do not simply scale with
376 temperature or precipitation (Dawson et al., 2013; Tai et al., 2010).

377 For each region and ensemble member, we construct probability density functions by
378 averaging PM_{2.5} over each region on every summer day for the first, middle, and last decade in the
379 RCP8.5_WMGG simulations. The degree to which the ensemble members in different time
380 periods separate from each other offers a measure of significance. GFDL-CM3 simulates decreases
381 in the number of days with low PM_{2.5} concentrations in favor of higher values over the Northeast,
382 Midwest, and Mid-Atlantic regions (light to darker to darkest curves in Figure 5). Little detectable
383 change occurs over the East Texas and Southeast regions as the ensemble members overlap in all
384 three time periods (Figure 5). CESM1 does not project significant changes although a shift towards
385 higher values is perceptible over the Northeast (Figure S7). Overall, this analysis indicates that the

386 uncertainty arising from differences in the model responses to climate change (structural
 387 uncertainty) exceeds that from internal variability.



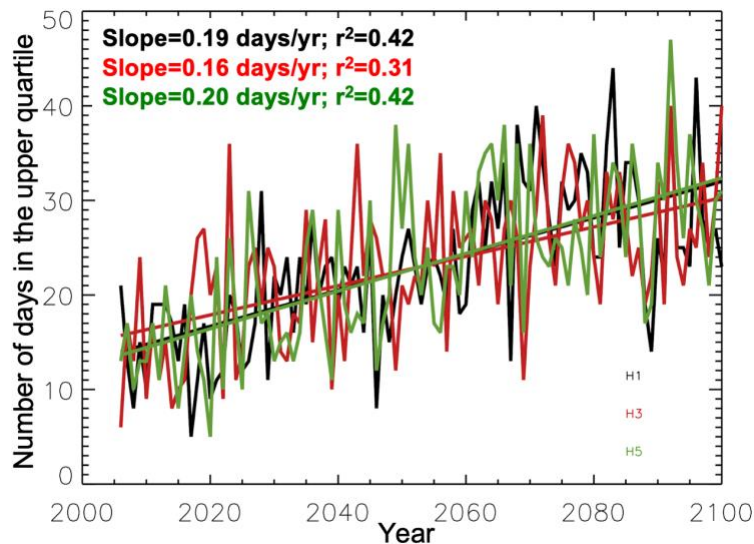
388

389 **Figure 5.** Increasing frequency of high PM_{2.5} events under the RCP8.5_WMGG climate scenario
 390 in the GFDL-CM3 model over much of the EUS. Average number of summer days with daily
 391 PM_{2.5} falling within 2 µg m⁻³ concentration bins, regionally averaged (where EOF loading > 0.5 in
 392 Figure 1) in each GFDL CM3 ensemble member for the years 2006-2015 (light), 2051-2060
 393 (darker) and 2091-2100 (darkest).

394 4.2 High-PM_{2.5} events: Frequency, duration and intensity

395 We illustrate our approach with the GFDL-CM3 Northeast EOF for PM_{2.5}. We select the
 396 upper quartile defined by the full 2006-2100 time series (all values above the red line in Figure
 397 S8) and count, separately for each ensemble member, the number of summer days when PM_{2.5}
 398 falls in the upper quartile. Over the 21st century, all three GFDL-CM3 ensemble members simulate
 399 an increase in this statistic (Figure 6). An ordinary least squares regression suggests an increase
 400 in the number of summer days with PM_{2.5} concentrations falling in the upper quartile of 16-20 days
 401 ($r^2 = 0.3-0.4$; range is across ensemble members) by end-of-century. While the changes are not
 402 linear with time, this simple metric enables a comparison of changing event frequency over time

403 across ensemble members and variables. Table S4 reports the GFDL-CM3 ensemble mean of these
 404 regression statistics for high-PM events, as well as ozone and temperature, in all five regions.

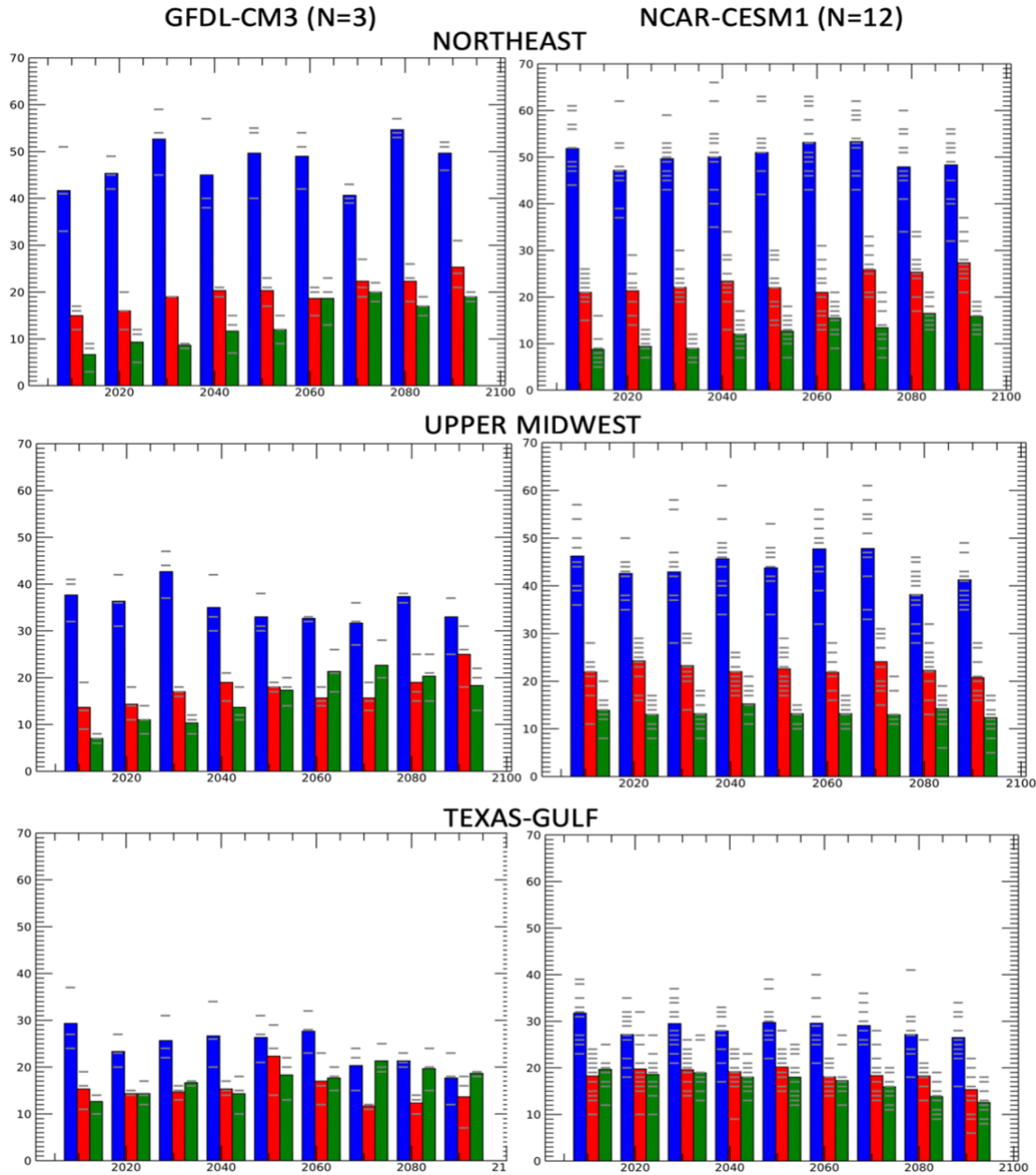


405

406 **Figure 6.** Number of summer days with daily $PM_{2.5}$ falling within the upper quartile defined with
 407 respect to the full 2006-2100 period, separately for each GFDL-CM3 ensemble member (colors).
 408 Slopes and coefficients of determination (r^2) from ordinary least squares regression are shown in
 409 the panel.

410 To assess changes in the duration of high $PM_{2.5}$ events, we define short (1-2 day), medium
 411 (3-4 day) and long (5+ days) durations of top quartile summertime $PM_{2.5}$ events by tracking the
 412 number of successive days the PC stays in the upper quartile. For each decade, we sum over all
 413 short, medium, and long events. We then average across all ensemble members and report the
 414 ensemble mean number of events per decade (colored bars in Figures 7 and S9). Anthropogenic
 415 climate change increases the number of 5+ day events over the 21st century, in all regions (green
 416 bars in Figures 7 and S9) in GFDL-CM3, although not all changes are significant relative to
 417 internal variability (Section 4.3). CESM1 also shows a 21st century increase in 5+ day Northeast
 418 $PM_{2.5}$ events but simulates little change or an ensemble average decrease in the longest duration
 419 events over other regions (Figures 7 and S9). The differences between the two models in the

420 simulated number of long-lasting events are generally of the same sign as the differences between
 421 the simulated summertime mean PM_{2.5} changes in Figure 4.

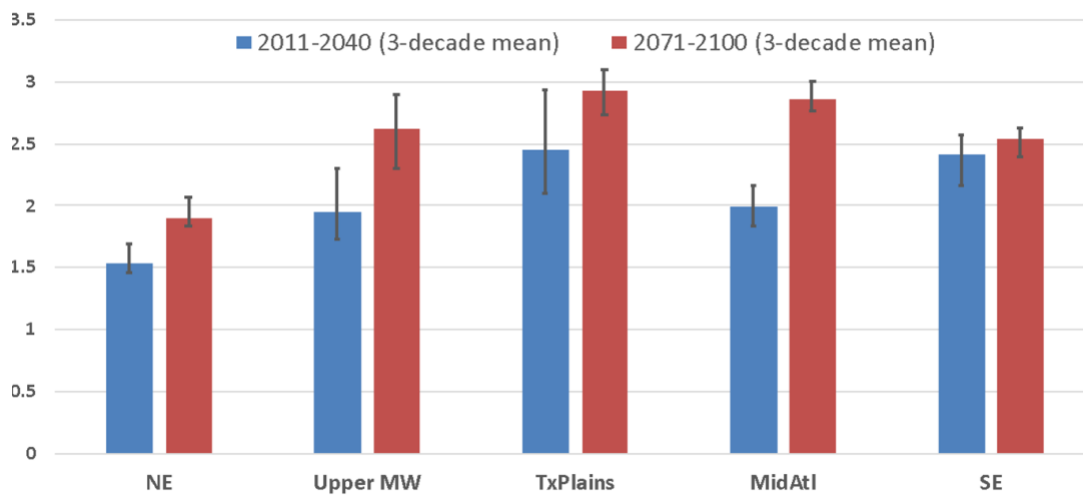


422

423 **Figure 7.** Longer duration upper quartile regional-scale PM_{2.5} events occur under the
 424 RCP8.5_WMGG scenario in some regions in the GFDL-CM3 model, but only over the Northeast,
 425 and to a lesser extent in CESM1. Shown are the number of times the PC derived from daily mean
 426 PM_{2.5} exceeds the upper quartile value, calculated from the full 2006-2100 time period, and stays
 427 above that value for 1-2 (blue), 3-4 (red), or 5+ (green) days, summed over each decade within
 428 each ensemble member prior to averaging over all GFDL-CM3 (left) and NCAR-CESM1 (right)
 429 ensemble members (N) over the Northeast (top), Upper Midwest (middle) and East Texas (bottom)
 430 under the RCP8.5_WMGG scenario. The decadal sums for each individual ensemble member are

431 shown as gray horizontal lines. The range across the gray lines for a given decade is a measure of
 432 internal variability. A forced response to rising greenhouse gases is ‘detected’ when all of the gray
 433 lines in a later decade emerge from the range in the early decades.

434 Our approach thus far defines the upper quartile across the whole time series, which could
 435 diagnose a change in duration solely because the frequency changed. Such a change in duration
 436 is still relevant from a health impact perspective, especially if extended duration events trigger
 437 non-linear health responses. We also investigate the extent to which duration has changed
 438 independently from frequency, such as may occur from changing atmospheric circulation. We
 439 sample the 10 days each summer with the highest intensity pollution events in GFDL-CM3. We
 440 then calculate an average length of episode over the first three vs last three decades of the 21st
 441 century. Figure 8 implies that much of the change occurring in Figure 7 is due to changes in
 442 frequency. A lengthening of over 0.5 days in the Midwest and almost a full day over the Mid-
 443 Atlantic may suggest some underlying fundamental change in ventilation, such as a northward
 444 shift of the summertime mid-latitude jet (Barnes & Fiore, 2013; Kerr et al., 2020).



445
 446 **Figure 8.** Average length of regional-scale (EOF regions from Figure 1) summertime PM_{2.5} events
 447 in the beginning (blue; 2011-2040) versus end (red; 2071-2100) of the 21st century in the GFDL-
 448 CM3 model, sampled from 10 days each summer with the highest PM_{2.5} concentrations. The
 449 vertical bars indicate the range across the three ensemble members.

450 As a means of gauging changes in the ‘intensity’ of events, we construct regional averages
 451 of daily PM_{2.5} over the five regions in Figure 1 (where EOF1 loadings > 0.5) and report the
 452 ensemble mean changes in both models during the 21st century in Table S5. Ensemble mean
 453 increases occur in this statistic across all time periods and regions within the GFDL-CM3 model.
 454 In CESM1, the ensemble mean increases only over the Northeast, with a slight increase in the
 455 upper Midwest by mid-century. We explore the range across individual ensemble members in the
 456 next section.

457 4.3 Changing regional high-PM_{2.5} events in the context of internal climate variability

458 A novel aspect of our analysis is the use of multiple ensemble members to gauge the
 459 significance of changes in high pollution events in light of the variability that arises naturally

460 (internally) in the climate system. The gray lines in Figure 7 denote individual ensemble members
461 (3 GFDL-CM3; 12 NCAR-CESM1). We first consider changes to be significant from one period
462 to another if all ensemble members in the later period fall outside the range of values from the
463 earlier period. GFDL-CM3 simulates significant changes in the longest duration (5+ day) events
464 between the first three and last three decades of the 21st century over the Northeast and mid-
465 Atlantic, and between the first and last two decades of the 21st century in the Southeast (Figures 7
466 and S9). While the ensemble mean suggests increases in the longest duration events between the
467 early and late 21st century over East Texas and the Upper Midwest (Figure 7), the ensemble
468 member ranges in early versus late decades overlap, implying that these changes are not fully
469 emerging from those that might arise solely due to internal climate variability. While CESM1
470 indicates a tendency towards increases in the number of 5+ day events, unlike the 3-member
471 GFDL-CM3 ensemble, the ranges across ensemble members in the last few decades do not fully
472 separate from the ranges in the first few decades, even over the Northeast. With a sufficiently large
473 ensemble, such as the multi-model 100-member ensembles now being generated for physical
474 climate models, one could better quantify the probability that these changes could arise solely from
475 climate variability, and more cleanly separate inter-model differences from climate variability.

476 To explore the range of changes one might have diagnosed with a 3-member ensemble
477 as compared to a 12-member ensemble, we consider two end-member cases by comparing the
478 simulated changes in PM_{2.5} event duration from the first two to the last two decades of the 21st
479 century diagnosed by sampling only six of the NCAR-CESM1 ensemble members: three with the
480 smallest (or largest decreases) or largest increases in PM_{2.5}. We aim to demonstrate the range that
481 might have occurred if we only had 3 members available, as a way to gauge the potential variability
482 we might have sampled with a larger GFDL-CM3 ensemble. For the longest duration events over
483 the Northeast, increases from the beginning to end-of-century range from 4 to 9.5 days across
484 individual NCAR-CESM1 ensemble members, with the three smallest averaging an increase of
485 4.2 events per decade that last 5+ days, and the three largest ensemble members averaging an
486 increase of 9.5. For 3-4 day events in the Northeast, the full range spans a decrease of 0.5 to an
487 increase of 11 events, while the averages of the three smallest versus largest ensemble members
488 are 0.83 and 9.5, respectively. We conclude that our limited sampling of three ensemble members
489 in GFDL-CM3 is likely under-representing internal variability, leading to over-confident detection
490 of significant changes in Figure 7.

491 An analysis of maximum and minimum changes in the 75th percentile daily mean
492 summertime PM_{2.5} values reveals that structural (model response) uncertainty outweighs the role
493 of climate variability (Table S5). The range of changes simulated by the 3-member GFDL
494 ensemble lies completely outside that of the 12-member NCAR ensemble for the Northeast,
495 Midwest, and Mid-Atlantic regions. All three GFDL ensemble members simulate increasing 75th
496 percentile values across all regions except for the East Texas region at mid-Century. In contrast,
497 the sign of the change simulated by CESM1 is only consistent across all 12 ensemble members for
498 the Northeast (increase) and Mid-Atlantic (decrease) by end of century (recall that the mid-Atlantic
499 EOF is displaced inland in CESM1 with respect to observations, Figure 1).

500 We also select the three NCAR-CESM1 ensemble members with either the smallest or
501 largest changes in 75th percentile daily mean summertime PM_{2.5} concentrations (Table S5). Nearly
502 a factor of 3 range occurs if one considers the average of the 3 NCAR-CESM1 ensemble members
503 with the smallest versus the largest simulated changes over the Northeast. We conclude that inter-

504 model discrepancies reported in the published literature regarding the sign and magnitude of the
505 PM_{2.5} response to climate change reflect not only model structural differences but also internally
506 arising climate variability. This ‘climate noise’ could be quantified with sufficiently large
507 ensembles that isolate the anthropogenic climate change “signal” (ensemble mean) from the
508 “noise” (ensemble range). Multi-model large ensembles can further distinguish inter-model
509 differences (structural or model response uncertainty) from internal variability (Deser et al., 2020).

510 **5 PM_{2.5}-O₃-Temperature Linkages Within and Across Regions**

511 The observational analysis of Schnell and Prather (2017) indicates that extreme events in
512 temperature, MDA8 O₃ and daily mean PM_{2.5} often occur within about a day of each other across
513 the EUS, but the specific relationships vary by region. Climate change induced by rising long-
514 lived greenhouse gases does not change the regional-scale modes of variability in PM_{2.5}, O₃, or
515 daily T_{max} as the patterns remain similar throughout the 21st century (Figure S2). Table 1 shows
516 relationships between the 2006-2100 PCs derived from GFDL-CM3 MDA8 O₃, daily mean PM_{2.5}
517 and daily T_{max} within each region. We also examine changes in these relationships over the 21st
518 century by separately analyzing correlations for two decades in the beginning (2006-2025) versus
519 end (2081-2100) of the simulations. The timing of the strongest correlations in Table 1, derived
520 from the daily summertime PCs, are broadly consistent with those emerging from analysis of the
521 95th percentile of observed warm season pollution and temperature events by Schnell and Prather
522 (2017; see their Figure 4DEF), despite our use of a different metric.

523 Over all regions and time periods, the strongest correlations in GFDL-CM3 emerge for PM_{2.5}
524 lagging MDA8 O₃ by a day. Future work is needed to determine if these relationships are solely
525 governed by meteorological processes or if, for instance, enhanced O₃ (and OH) production on
526 one day contributes to secondary aerosol formation that accumulates to high PM_{2.5} levels the
527 following day. While secondary inorganic aerosol formation is represented in our GFDL-CM3
528 configuration, the treatment of secondary organic aerosol is highly simplified and biogenic
529 emissions do not respond to meteorology. Along with the increase in upper quartile PM_{2.5} events
530 discussed in Section 4.2, GFDL-CM3 also projects more frequent O₃ events in both the Northeast
531 and the Mid-Atlantic as well as heat events (Table S4). All three GFDL-CM3 ensemble members
532 show that PM_{2.5}-O₃ correlations strengthen or remain similar from 2006-2025 to 2081-2100, with

533 the largest ensemble mean increases occurring over the Southeast (r increases by 0.09) and East
 534 Texas (r increases by 0.13) regions.

REGION	T_{\max} and O_3			T_{\max} and PM			O_3 and PM		
	Lag -1	Lag 0	Lag +1	Lag -1	Lag 0	Lag +1	Lag -1	Lag 0	Lag +1
<i>Over all summers of 2006-2100</i>									
Northeast	0.47	0.50	0.38	0.48	0.57	0.57	0.25	0.58	0.71
Mid-Atlantic	0.67	0.67	0.58	0.33	0.37	0.37	0.40	0.57	0.65
Upper Midwest	0.59	0.54	0.39	0.51	0.56	0.51	0.36	0.61	0.71
East Texas	0.03	-0.01	-0.02	0.05	0.04	0.02	0.34	0.51	0.61
Southeast	0.03	-0.01	-0.01	0.16	0.15	0.14	0.27	0.46	0.49
<i>Only summers of 2006-2025</i>									
Northeast	0.56	0.59	0.42	0.52	0.65	0.63	0.26	0.58	0.72
Mid-Atlantic	0.71	0.71	0.59	0.26	0.34	0.33	0.33	0.51	0.60
Upper Midwest	0.70	0.62	0.42	0.50	0.57	0.49	0.31	0.58	0.71
East Texas	0.12	0.06	0.04	-0.02	-0.05	-0.08	0.26	0.44	0.55
Southeast	0.00	-0.05	-0.04	0.07	0.05	0.04	0.23	0.42	0.45
<i>Only summers of 2081-2100</i>									
Northeast	0.39	0.42	0.29	0.45	0.55	0.55	0.19	0.55	0.70
Mid-Atlantic	0.60	0.60	0.51	0.26	0.31	0.30	0.39	0.57	0.64
Upper Midwest	0.53	0.47	0.31	0.50	0.56	0.49	0.31	0.58	0.68
East Texas	0.00	-0.02	0.00	-0.01	-0.01	-0.03	0.45	0.61	0.68
Southeast	0.06	0.03	0.03	0.17	0.17	0.16	0.32	0.51	0.54

535 **Table 1.** Ensemble mean correlation coefficients (r) between principal components for pairs of
 536 variables simulated by the GFDL-CM3 model (T_{\max} is daily maximum temperature at a 2m
 537 reference height; O_3 is MDA8 O_3 ; PM is daily mean $PM_{2.5}$). Correlations are reported for each
 538 region on the same day (Lag 0) or with the first variable lagging (Lag -1) or leading (Lag +1) by
 539 one day. Correlations are taken for each individual ensemble member prior to averaging. The
 540 strongest correlation for each pair of variables is shown in bold where $r \geq 0.45$.

541 The correlation of temperature with O_3 is strongest for zero lag (same day) in the Northeast,
 542 and for the same day or O_3 preceding temperature by a day over the Mid-Atlantic, and when ozone
 543 precedes temperature by a day over the Upper Midwest. GFDL-CM3 projects a weakening of this
 544 temperature- O_3 correlation over the 21st century, with ensemble mean decreases of $r=0.17$, 0.11,
 545 and 0.17 for the Northeast, Mid-Atlantic, and Upper Midwest, respectively. The degraded
 546 correlation between O_3 and temperature under climate change was previously shown to occur in
 547 this model, and attributed to the summertime mid-latitude jet shifting northward (Barnes & Fiore,
 548 2013). We find no correlation in either of the southern regions (East Texas and Southeast) between
 549 temperature and O_3 . The absence of an O_3 -temperature relationship in GFDL-CM3 agrees with
 550 earlier observation-based work showing that humidity offers more explanatory power for O_3 in

551 these regions (Camalier et al., 2007), possibly reflecting a key role for land-atmosphere couplings
552 (Kavassalis & Murphy, 2017; Tawfik & Steiner, 2013).

553 For temperature and PM_{2.5}, we additionally draw on the NCAR-CESM1 simulations. Both
554 models simulate the strongest correlations with zero lag (Tables 1 and S6). All NCAR-CESM1
555 ensemble members simulate the strongest PM-temperature correlations over the Northeast
556 (ensemble mean $r = 0.58$, with a range of $r=0.55$ to 0.60 ; Table S6), but unlike GFDL-CM3, PM_{2.5}
557 and temperature are not correlated over the displaced Mid-Atlantic region in CESM1 even though
558 an EOF analysis of the CESM1 daily summertime temperature fields reveals a similarly shifted
559 pattern as for PM_{2.5} (Figure S1b). While GFDL-CM3 simulates no relationship between
560 temperature and PM_{2.5} in either southern region, CESM1 indicates a weak temperature-PM_{2.5}
561 anticorrelation for East Texas (Table S6). Prior observation-based work has demonstrated more
562 complex relationships between PM_{2.5} and meteorology (Dawson et al., 2013), in part because
563 individual PM_{2.5} components display different relationships with meteorological variables (Tai et
564 al., 2010; X. Wu et al., 2019). For the highest observed EUS summertime PM_{2.5} events, however,
565 strong relationships with temperature have been found (Porter et al., 2015). The Northeast is the
566 only region for which we identify a consistent change in the PM_{2.5}-T relationship across the three
567 GFDL ensemble members from 2006-2025 to 2081-2100, where the correlation declines by an
568 ensemble average of $r=0.10$ (Table 1).

569 At present, the EUS climatological summertime near-surface winds are associated with the large-
570 scale circulation around the North Atlantic Subtropical High system, with southerly flow across
571 the southern portion of the domain becoming southwesterly or westerly to the north. A simple
572 inter-regional correlation analysis for MDA8 O₃ and daily mean PM_{2.5} (Table S7) implies a
573 continuation of this circulation pattern over the course of the century. The Northeast and Mid-
574 Atlantic PCs for both air pollutants correlate most strongly with zero lag ($r \sim 0.5$) whereas both
575 regions tend to lag the Upper Midwest PC by a day ($r \sim 0.7$). The East Texas and Southeast PCs
576 for O₃ and PM correlate most strongly on the same day ($r \sim 0.5, 0.6$, respectively), and the Upper
577 Midwest PM PCs correlate most strongly with the East Texas region when lagged by a day ($r \sim$
578 0.5). In contrast, the inter-regional correlations for the temperature PCs are almost always strongest
579 for zero lag (not shown). We also conduct this inter-regional correlation analysis separately for
580 simulation years 2006-2025 versus 2081-2100 in each of the 3 GFDL-CM3 ensemble members,
581 but do not detect any robust changes over the course of the century.

582 **6 Discussion and Conclusions**

583 Prior work has shown that some regions experiencing high pollution levels at present will
584 suffer from additional degradation of air quality as the planet continues to warm, if additional
585 controls on air pollutant emissions are not implemented. These studies, however, often conflict
586 (Fiore et al., 2015; Jacob & Winner, 2009; Weaver et al., 2009) and have typically neglected the
587 role of naturally arising internal climate variability by simulating only a small number of years
588 (Deser et al., 2012ab; Garcia-Menendez et al., 2017; Hawkins & Sutton, 2009). With initial
589 condition ensembles in the GFDL-CM3 and CESM1 climate models under a 21st century RCP8.5
590 scenario with air pollutant emissions frozen in 2005 (denoted RCP8.5_WMGG), we estimate
591 uncertainty due to internal climate variability as the range across the ensemble members available
592 from each model. Relative to this internal variability, we evaluate long-term trends in mean and

593 high air pollution events driven by rising greenhouse gases, as well as model response differences.
594 Differences between the two models serve as a measure of model response (structural) uncertainty.

595 We demonstrate how Empirical Orthogonal Function (EOF) analysis can be applied to quantify
596 changes in both the frequency and duration of summertime regional-scale pollution episodes over
597 the Eastern United States (EUS). By revealing underlying spatiotemporal patterns of variability,
598 this statistical approach avoids the challenge of bias-correcting individual models, which would
599 be necessary if we were to define high pollution events using an absolute concentration threshold.
600 We find that the models agree best over the Northeast region, where summertime mean surface
601 temperatures increase by over 5 °C during this century, accompanied by a rise in summertime
602 mean PM_{2.5} (up to 1-4 µg m⁻³). Our analysis of principal components (PCs), the time series
603 accompanying each EOF that indicates how strongly expressed each spatial pattern is on each
604 summer day, reveals an increase in the decadal incidence of upper quartile PM_{2.5} events lasting at
605 least five days over the Northeast that is significant relative to climate variability in GFDL-CM3,
606 and bordering on significant in CESM1 (Figure 7).

607 The GFDL-CM3 simulations capture, at least qualitatively, observed temporal relationships
608 between EUS MDA8 O₃, daily average PM_{2.5}, and daily T_{max}, including those identified by Schnell
609 and Prather (2017). The close temporal occurrence of O₃ and PM_{2.5}, and in some cases temperature,
610 events could be relevant to public health, particularly if non-linear responses occur from
611 consecutive or simultaneous exposure. Same-day and consecutive-day exposure to O₃ and PM_{2.5}
612 occurs across the EUS, with GFDL-CM3 projecting a strengthening of this correlation in the
613 southern EUS during the 21st century. Correlated extremes of air pollution and temperature may
614 become more relevant for public health in future decades, particularly in the northern part of our
615 domain where both O₃ and PM_{2.5} remain correlated with temperature (Table 1) and where the
616 frequency and duration of events may increase (Figures 7 and 8). Mascioli et al. (2016) showed
617 that GFDL-CM3 simulates daily T_{max} in excess of the 90th percentile defined relative to 1961-1990
618 for nearly the entire summer by the 2090s in the RCP8.5 scenario. This standard RCP8.5 scenario
619 warms even more than RCP8.5_WMGG because global aerosols decline, removing the net cooling
620 influence from aerosols, while air quality improves.

621 The changes we diagnose from GFDL-CM3 imply a trend towards longer-lasting exposures to
622 high pollution events, which may have implications for human and plant health, particularly when
623 accompanied by more intense heat events. By holding anthropogenic emissions fixed in our
624 scenario, we do not consider the potential for human activities to exacerbate or mitigate air
625 pollution levels. This major source of uncertainty has been emphasized in prior studies assessed in
626 Intergovernmental Panel on Climate Change reports (*e.g.*, Kirtman et al., 2013). While we focused
627 on summertime, climate change may extend what is currently ‘summer’ weather and the
628 accompanying pollutant levels over the EUS into spring and fall, as occurred in October 2010 over
629 the Southeast, triggering high fire and biogenic emissions (Y. Zhang & Wang, 2016). Our study
630 focused on the response of air pollution to changes in meteorology under rising greenhouse gases.
631 Weather-sensitive emission feedbacks such as from wildfires and biogenic emissions were not
632 included in our simulations, and would most likely further amplify pollutant exposure of
633 vulnerable populations and vegetation.

634 The 12-member NCAR-CESM1 ensemble provides a broader sampling of possible climate
635 states than the 3-member GFDL-CM3 ensemble. Outside of the Northeast, CESM1 simulates

636 different changes in summertime mean PM_{2.5} and upper quartile events, and we find that in some
637 regions, the models do not overlap in their simulated 21st century changes. While three ensemble
638 members is a poor sampling of climate variability, the discrepancies between the two models are
639 sufficiently large as to imply fundamental model differences in their climate responses to rising
640 greenhouse gases. As emphasized by Hawkins & Sutton (2009), uncertain model responses have
641 the potential to be reduced by advancing process-level understanding and improving its
642 representation in models. Air quality projections produced with multi-model chemistry-climate
643 ensembles could transform the capacity to develop probabilistic assessments of changes in
644 regional-scale pollution event frequency and duration, and their co-occurrence with heat, as well
645 as any other metrics of interest for public health or ecosystem welfare. Such ensembles can be
646 parsed separately for uncertainty arising from climate variability versus different model responses.

647 Our EOF-based approach can be readily applied to any future single or multi-model initial
648 condition chemistry-climate model ensembles. For example, future simulations could sample a
649 wide range of scenarios and incorporate potentially important feedbacks that were neglected in our
650 simulations. A more immediate direction could link EOF patterns to specific meteorological
651 conditions, in which case one could probe existing multi-model initial-condition physical climate
652 model ensembles, with as many as 100 members per model already available (C. Deser et al.,
653 2020), for insights into projected changes in daily MDA8 O₃ and PM_{2.5} events. Understanding and
654 preparing for the range of changes in pollution events that could arise from climate variability may
655 be as important as quantifying the signal from climate change, particularly if climate mitigation
656 leads to less extreme warming scenarios for the 21st century than simulated here.

657 **Acknowledgments, Samples, and Data**

658 We are grateful for helpful discussions with Drs. Dan Bishop, Ron Cohen, Louisa Emmons, Larry
659 Horowitz, Lee Murray, Vaishali Naik, Michael Previdi and Dan Westervelt. We acknowledge
660 Johnny Lin for his publicly available IDL code for varimax rotation [varimax_k58.pro](#). This article
661 was developed under Assistance Agreements 83520601 and 83587801 awarded by the U.S.
662 Environmental Protection Agency to A.M. Fiore. It has not been formally reviewed by EPA. The
663 views expressed in this document are solely those of the authors and do not necessarily reflect
664 those of the Agency. EPA does not endorse any products or commercial services mentioned in
665 this publication. The CESM project is supported primarily by the National Science Foundation
666 (NSF). This material is based upon work supported by the National Center for Atmospheric
667 Research (NCAR), which is a major facility sponsored by the NSF under Cooperative Agreement
668 1852977. Data and code used to create figures will be provided in Columbia University Academic
669 Commons at

670 **References**

- 671 Abatzoglou, J. T., & Williams, A. P. (2016). Impact of anthropogenic climate change on wildfire
672 across western US forests. *Proceedings of the National Academy of Sciences*, 113(42), 11770-
673 11775. <https://www.pnas.org/content/pnas/113/42/11770.full.pdf>
- 674 Andersson, C., & Engardt, M. (2010). European ozone in a future climate: Importance of
675 changes in dry deposition and isoprene emissions. *J. Geophys. Res.*, 115(D2), D02303.
676 <http://dx.doi.org/10.1029/2008JD011690>

- 677 Austin, J., Horowitz, L. W., Schwarzkopf, M. D., Wilson, R. J., & Levy, H. (2013). Stratospheric
678 Ozone and Temperature Simulated from the Preindustrial Era to the Present Day. *Journal of*
679 *Climate*, 26(11), 3528-3543. <http://dx.doi.org/10.1175/JCLI-D-12-00162.1>
- 680 Barnes, E. A., & Fiore, A. M. (2013). Surface ozone variability and the jet position: Implications
681 for projecting future air quality. *Geophysical Research Letters*, 40(11), 2839-2844.
682 <http://dx.doi.org/10.1002/grl.50411>
- 683 Bowden, J. H., Nolte, C. G., & Otte, T. L. (2013). Simulating the impact of the large-scale
684 circulation on the 2-m temperature and precipitation climatology. *Climate Dynamics*, 40(7),
685 1903-1920. <https://doi.org/10.1007/s00382-012-1440-y>
- 686 Boys, B. L., Martin, R. V., van Donkelaar, A., MacDonell, R. J., Hsu, N. C., Cooper, M. J., et al.
687 (2014). Fifteen-Year Global Time Series of Satellite-Derived Fine Particulate Matter.
688 *Environmental Science & Technology*, 48(19), 11109-11118. <https://doi.org/10.1021/es502113p>
- 689 Camalier, L., Cox, W., & Dolwick, P. (2007). The effects of meteorology on ozone in urban
690 areas and their use in assessing ozone trends. *Atmospheric Environment*, 41(33), 7127-7137.
691 [http://www.sciencedirect.com/science/article/B6VH3-4NR18M7-](http://www.sciencedirect.com/science/article/B6VH3-4NR18M7-2/2/96f87a4d98435ecbf7fd411e2ee1fa4e)
692 [2/2/96f87a4d98435ecbf7fd411e2ee1fa4e](http://www.sciencedirect.com/science/article/B6VH3-4NR18M7-2/2/96f87a4d98435ecbf7fd411e2ee1fa4e)
- 693 Clifton, O. E., Fiore, A. M., Correa, G., Horowitz, L. W., & Naik, V. (2014). Twenty-first
694 century reversal of the surface ozone seasonal cycle over the northeastern United States.
695 *Geophysical Research Letters*, 41(20), 7343-7350.
696 <https://agupubs.onlinelibrary.wiley.com/doi/abs/10.1002/2014GL061378>
- 697 Coffel, E. D., Horton, R. M., & de Sherbinin, A. (2017). Temperature and humidity based
698 projections of a rapid rise in global heat stress exposure during the 21st century. *Environmental*
699 *Research Letters*, 13(1), 014001. <http://dx.doi.org/10.1088/1748-9326/aaa00e>
- 700 Cooper, O. R., Gao, R.-S., Tarasick, D., Leblanc, T., & Sweeney, C. (2012). Long-term ozone
701 trends at rural ozone monitoring sites across the United States, 1990–2010. *Journal of*
702 *Geophysical Research: Atmospheres*, 117(D22), D22307.
703 <http://dx.doi.org/10.1029/2012JD018261>
- 704 Dawson, J. P., Bloomer, B. J., Winner, D. A., & Weaver, C. P. (2013). Understanding the
705 meteorological drivers of U.S. particulate matter concentrations in a changing climate. *Bulletin*
706 *of the American Meteorological Society*. <http://dx.doi.org/10.1175/BAMS-D-12-00181.1>
- 707 Deser, C., Knutti, R., Solomon, S., & Phillips, A. S. (2012a). Communication of the role of
708 natural variability in future North American climate. *Nature Clim. Change*, 2(12), 888-888.
709 10.1038/nclimate1779. <http://dx.doi.org/10.1038/nclimate1779>
- 710 Deser, C., Lehner, F., Rodgers, K. B., Ault, T., Delworth, T. L., DiNezio, P. N., et al. (2020).
711 Insights from Earth system model initial-condition large ensembles and future prospects. *Nature*
712 *Climate Change*, 10(4), 277-286. <https://doi.org/10.1038/s41558-020-0731-2>
- 713 Deser, C., Phillips, A. S., Alexander, M. A., & Smoliak, B. V. (2013). Projecting North
714 American Climate Over the Next 50 Years: Uncertainty due to Internal Variability. *Journal of*
715 *Climate*. <http://dx.doi.org/10.1175/JCLI-D-13-00451.1>

- 716 Deser, C., Phillips, A., Bourdette, V., & Teng, H. (2012b). Uncertainty in climate change
 717 projections: the role of internal variability. *Climate Dynamics*, 38(3-4), 527-546.
 718 <http://dx.doi.org/10.1007/s00382-010-0977-x>
- 719 Donner, L. J., Wyman, B. L., Hemler, R. S., Horowitz, L. W., Ming, Y., Zhao, M., et al. (2011).
 720 The Dynamical Core, Physical Parameterizations, and Basic Simulation Characteristics of the
 721 Atmospheric Component AM3 of the GFDL Global Coupled Model CM3. *Journal of Climate*,
 722 24(13), 3484-3519. <http://dx.doi.org/10.1175/2011JCLI3955.1>
- 723 East, J., & Garcia-Menendez, F. (2020). Internal climate variability and initial condition
 724 ensembles in air quality projections. *U.S. CLIVAR Variations* (Summer 2020, 18, No. 2).
 725 <https://opensky.ucar.edu/islandora/object/usclivar:125>
- 726 Eder, B. K., Davis, J. M., & Bloomfield, P. (1993). A characterization of the spatiotemporal
 727 variability of non-urban ozone concentrations over the eastern United States. *Atmospheric*
 728 *Environment. Part A. General Topics*, 27(16), 2645-2668.
 729 <http://www.sciencedirect.com/science/article/pii/096016869390035W>
- 730 Filleul, L., Cassadou, S., Médina, S., Fabres, P., Lefranc, A., Eilstein, D., et al. (2006). The
 731 relation between temperature, ozone, and mortality in nine French cities during the heat wave of
 732 2003. *Environmental Health Perspectives*, 114(9), 1344-1347.
 733 <https://pubmed.ncbi.nlm.nih.gov/16966086>
- 734 Fiore, A. M., Jacob, D. J., Mathur, R., & Martin, R. V. (2003). Application of empirical
 735 orthogonal functions to evaluate ozone simulations with regional and global models. *J. Geophys.*
 736 *Res.*, 108(D14), 4431. <http://dx.doi.org/10.1029/2002JD003151>
- 737 Fiore, A. M., Naik, V., & Leibensperger, E. M. (2015). Air Quality and Climate Connections.
 738 *Journal of the Air & Waste Management Association*, 65(6), 645-685.
 739 <https://doi.org/10.1080/10962247.2015.1040526>
- 740 Fiore, A. M., Naik, V., Spracklen, D. V., Steiner, A., Unger, N., Prather, M., et al. (2012). Global
 741 air quality and climate. *Chemical Society Reviews*, 41(19), 6663-6683.
 742 <http://dx.doi.org/10.1039/C2CS35095E>
- 743 Frost, G. J., McKeen, S. A., Trainer, M., Ryerson, T. B., Neuman, J. A., Roberts, J. M., et al.
 744 (2006). Effects of changing power plant NO_x emissions on ozone in the eastern United States:
 745 Proof of concept. *Journal of Geophysical Research: Atmospheres*, 111(D12), D12306.
 746 <http://dx.doi.org/10.1029/2005JD006354>
- 747 Fu, T.-M., & Tian, H. (2019). Climate Change Penalty to Ozone Air Quality: Review of Current
 748 Understandings and Knowledge Gaps. *Current Pollution Reports*, 5(3), 159-171.
 749 <https://doi.org/10.1007/s40726-019-00115-6>
- 750 García-Herrera, R., Díaz, J., Trigo, R. M., Luterbacher, J., & Fischer, E. M. (2010). A Review of
 751 the European Summer Heat Wave of 2003. *Critical Reviews in Environmental Science and*
 752 *Technology*, 40(4), 267-306. <https://doi.org/10.1080/10643380802238137>
- 753 Garcia-Menendez, F., Monier, E., & Selin, N. E. (2017). The role of natural variability in
 754 projections of climate change impacts on U.S. ozone pollution. *Geophysical Research Letters*,
 755 44(6), 2911-2921. <https://agupubs.onlinelibrary.wiley.com/doi/abs/10.1002/2016GL071565>

- 756 Ghan, S. J., Liu, X., Easter, R. C., Zaveri, R., Rasch, P. J., Yoon, J.-H., & Eaton, B. (2012).
757 Toward a Minimal Representation of Aerosols in Climate Models: Comparative Decomposition
758 of Aerosol Direct, Semidirect, and Indirect Radiative Forcing. *Journal of Climate*, 25(19), 6461-
759 6476. <https://doi.org/10.1175/JCLI-D-11-00650.1>
- 760 Hawkins, E., & Sutton, R. (2009). The Potential to Narrow Uncertainty in Regional Climate
761 Predictions. *Bulletin of the American Meteorological Society*, 1095-1108.
- 762 Hong, C., Zhang, Q., Zhang, Y., Davis, S. J., Tong, D., Zheng, Y., et al. (2019). Impacts of
763 climate change on future air quality and human health in China. *Proceedings of the National
764 Academy of Sciences*, 116(35), 17193-17200.
765 <https://www.pnas.org/content/pnas/116/35/17193.full.pdf>
- 766 Horton, D. E., Harshvardhan, & Diffenbaugh, N. S. (2012). Response of air stagnation frequency
767 to anthropogenically enhanced radiative forcing. *Environmental Research Letters*, 7(4), 044034.
768 <http://dx.doi.org/10.1088/1748-9326/7/4/044034>
- 769 Horton, D. E., Skinner, C. B., Singh, D., & Diffenbaugh, N. S. (2014). Occurrence and
770 persistence of future atmospheric stagnation events. *Nature Climate Change*, 4(8), 698-703.
771 <https://doi.org/10.1038/nclimate2272>
- 772 Hou, P., & Wu, S. (2016). Long-term Changes in Extreme Air Pollution Meteorology and the
773 Implications for Air Quality. *Scientific Reports*, 6(1), 23792. <https://doi.org/10.1038/srep23792>
- 774 Jacob, D. J., & Winner, D. A. (2009). Effect of climate change on air quality. *Atmospheric
775 Environment*, 43(1), 51-63. [http://www.sciencedirect.com/science/article/B6VH3-4TNWH49-
776 4/2/30b98e804a7d8cab841c22038bc0c264](http://www.sciencedirect.com/science/article/B6VH3-4TNWH49-4/2/30b98e804a7d8cab841c22038bc0c264)
- 777 Kavassalis, S. C., & Murphy, J. G. (2017). Understanding ozone-meteorology correlations: A
778 role for dry deposition. *Geophysical Research Letters*, 44(6), 2922-2931.
779 <https://agupubs.onlinelibrary.wiley.com/doi/abs/10.1002/2016GL071791>
- 780 Kay, J. E., Deser, C., Phillips, A., Mai, A., Hannay, C., Strand, G., et al. (2015). The Community
781 Earth System Model (CESM) Large Ensemble Project: A Community Resource for Studying
782 Climate Change in the Presence of Internal Climate Variability. *Bulletin of the American
783 Meteorological Society*, 96(8), 1333-1349. <https://doi.org/10.1175/BAMS-D-13-00255.1>
- 784 Kerr, G. H., Waugh, D. W., Steenrod, S. D., Strode, S. A., & Strahan, S. E. (2020). Surface
785 Ozone-Meteorology Relationships: Spatial Variations and the Role of the Jet Stream. *Journal of
786 Geophysical Research: Atmospheres*, 125(21), e2020JD032735.
787 <https://agupubs.onlinelibrary.wiley.com/doi/abs/10.1029/2020JD032735>
- 788 Kerr, G. H., Waugh, D. W., Strode, S. A., Steenrod, S. D., Oman, L. D., & Strahan, S. E. (2019).
789 Disentangling the Drivers of the Summertime Ozone-Temperature Relationship Over the United
790 States. *Journal of Geophysical Research: Atmospheres*, 124(19), 10503-10524.
791 <https://agupubs.onlinelibrary.wiley.com/doi/abs/10.1029/2019JD030572>
- 792 Kirtman, B., S.B. Power, J.A. Adedoyin, G.J. Boer, R. Bojariu, I. Camilloni, et al. (2013). Near-
793 term Climate Change: Projections and Predictability. In T. F. Stocker, D. Qin, G.-K. Plattner, M.
794 Tignor, S.K. Allen, J. Boschung, A. Nauels, Y. Xia, V. Bex, & P. M. Midgley (Eds.), *Climate
795 Change 2013: The Physical Science Basis. Contribution of Working Group I to the Fifth
796 Assessment Report of the Intergovernmental Panel on Climate Change*. Cambridge, United
797 Kingdom and New York, NY, USA: Cambridge University Press.

- 798 Konovalov, I. B., Beekmann, M., Kuznetsova, I. N., Yurova, A., & Zvyagintsev, A. M. (2011).
799 Atmospheric impacts of the 2010 Russian wildfires: integrating modelling and measurements of
800 an extreme air pollution episode in the Moscow region. *Atmos. Chem. Phys.*, *11*(19), 10031-
801 10056. <https://acp.copernicus.org/articles/11/10031/2011/>
- 802 Lamarque, J.-F., Kyle, G. P., Meinshausen, M., Riahi, K., Smith, S., van Vuuren, D., et al.
803 (2011). Global and regional evolution of short-lived radiatively-active gases and aerosols in the
804 Representative Concentration Pathways. *Climatic Change*, *109*(1-2), 191-212.
805 <http://dx.doi.org/10.1007/s10584-011-0155-0>
- 806 Lehman, J., Swinton, K., Bortnick, S., Hamilton, C., Baldrige, E., Eder, B., & Cox, B. (2004).
807 Spatio-temporal characterization of tropospheric ozone across the eastern United States.
808 *Atmospheric Environment*, *38*(26), 4357-4369.
809 <https://www.sciencedirect.com/science/article/pii/S1352231004003838>
- 810 Leibensperger, E. M., Mickley, L. J., & Jacob, D. J. (2008). Sensitivity of US air quality to mid-
811 latitude cyclone frequency and implications of 1980–2006 climate change. *Atmos. Chem. Phys.*,
812 *8*(23), 7075-7086. <http://www.atmos-chem-phys.net/8/7075/2008/>
813 <http://www.atmos-chem-phys.net/8/7075/2008/acp-8-7075-2008.pdf>
- 814 Li, L. F., Li, W. H., & Deng, Y. (2013). Summer rainfall variability over the Southeastern United
815 States and its intensification in the 21st century as assessed by CMIP5 models. *Journal of*
816 *Geophysical Research-Atmospheres*, *118*(2), 340-354. <Go to ISI>://000317838100008
- 817 Lin, C. Y. C., Jacob, D. J., & Fiore, A. M. (2001). Trends in exceedances of the ozone air quality
818 standard in the continental United States, 1980-1998. *Atmospheric Environment*, *35*(19), 3217-
819 3228. [http://www.sciencedirect.com/science/article/B6VH3-433W771-
820 1/2/4ee0c5d9076c1f8aad96415ff5cb353f](http://www.sciencedirect.com/science/article/B6VH3-433W771-1/2/4ee0c5d9076c1f8aad96415ff5cb353f)
- 821 Liu, X., Easter, R. C., Ghan, S. J., Zaveri, R., Rasch, P., Shi, X., et al. (2012). Toward a minimal
822 representation of aerosols in climate models: description and evaluation in the Community
823 Atmosphere Model CAM5. *Geosci. Model Dev.*, *5*(3), 709-739.
824 <https://gmd.copernicus.org/articles/5/709/2012/>
- 825 Logan, J. A. (1989). Ozone in Rural Areas of the United States. *J. Geophys. Res.*, *94*(D6), 8511-
826 8532.
- 827 Mascioli, N. R., Fiore, A. M., Previdi, M., & Correa, G. (2016). Temperature and Precipitation
828 Extremes in the United States: Quantifying the Responses to Anthropogenic Aerosols and
829 Greenhouse Gases, *Journal of Climate*, *29*(7), 2689-2701. Retrieved Jun 30, 2021, from
830 <https://journals.ametsoc.org/view/journals/clim/29/7/jcli-d-15-0478.1.xml>
- 831 Mickley, L. J., Jacob, D. J., Field, B. D., & Rind, D. (2004). Effects of future climate change on
832 regional air pollution episodes in the United States. *Geophys. Res. Lett.*, *31*(24), L24103.
833 <http://dx.doi.org/10.1029/2004GL021216>
- 834 Murphy, D. M., Chow, J. C., Leibensperger, E. M., Malm, W. C., Pitchford, M., Schichtel, B. A.,
835 et al. (2011). Decreases in elemental carbon and fine particle mass in the United States. *Atmos.*
836 *Chem. Phys.*, *11*(10), 4679-4686. <https://acp.copernicus.org/articles/11/4679/2011/>
- 837 Naik, V., Horowitz, L. W., Fiore, A. M., Ginoux, P., Mao, J., Aghedo, A. M., & Levy, H. (2013).
838 Impact of preindustrial to present-day changes in short-lived pollutant emissions on atmospheric

- 839 composition and climate forcing. *Journal of Geophysical Research: Atmospheres*, 118(14),
840 8086-8110. <http://dx.doi.org/10.1002/jgrd.50608>
- 841 Nolte, C. G., Spero, T. L., Bowden, J. H., Mallard, M. S., & Dolwick, P. D. (2018). The potential
842 effects of climate change on air quality across the conterminous US at 2030 under three
843 Representative Concentration Pathways. *Atmos. Chem. Phys.*, 18(20), 15471-15489.
844 <https://acp.copernicus.org/articles/18/15471/2018/>
- 845 Oswald, E. M., Dupigny-Giroux, L.-A., Leibensperger, E. M., Poirot, R., & Merrell, J. (2015).
846 Climate controls on air quality in the Northeastern U.S.: An examination of summertime ozone
847 statistics during 1993–2012. *Atmospheric Environment*, 112, 278-288.
848 <http://www.sciencedirect.com/science/article/pii/S1352231015300200>
- 849 Phalitnonkiat, P., Hess, P. G. M., Grigoriu, M. D., Samorodnitsky, G., Sun, W., Beaudry, E., et
850 al. (2018). Extremal dependence between temperature and ozone over the continental US. *Atmos.*
851 *Chem. Phys.*, 18(16), 11927-11948. <https://acp.copernicus.org/articles/18/11927/2018/>
- 852 Porter, W. C., & Heald, C. L. (2019). The mechanisms and meteorological drivers of the
853 summertime ozone–temperature relationship. *Atmos. Chem. Phys.*, 19(21), 13367-13381.
854 <https://www.atmos-chem-phys.net/19/13367/2019/>
- 855 Porter, W. C., Heald, C. L., Cooley, D., & Russell, B. (2015). Investigating the observed
856 sensitivities of air-quality extremes to meteorological drivers via quantile regression. *Atmos.*
857 *Chem. Phys.*, 15(18), 10349-10366. <https://www.atmos-chem-phys.net/15/10349/2015/>
- 858 Previdi, M., & Fiore, A. M. (2019). The Importance of Sampling Variability in Assessments of
859 ENSO-PM2.5 Relationships: A Case Study for the South Central United States. *Geophysical*
860 *Research Letters*, 46(12), 6878-6884.
861 <https://agupubs.onlinelibrary.wiley.com/doi/abs/10.1029/2019GL082250>
- 862 Rao, S. T., Zalewsky, E., & Zurbenko, I. G. (1995). Determining Temporal and Spatial
863 Variations in Ozone Air Quality. *Journal of the Air & Waste Management Association*, 45(1),
864 57-61. <https://doi.org/10.1080/10473289.1995.10467342>
- 865 Rieder, H. E., Fiore, A. M., Horowitz, L. W., & Naik, V. (2015). Projecting policy-relevant
866 metrics for high summertime ozone pollution events over the Eastern United States due to
867 climate and emission changes during the 21st century. *Journal of Geophysical Research:*
868 *Atmospheres*, 2014JD022303. <http://dx.doi.org/10.1002/2014JD022303>
- 869 Schmidt, D. F., & Grise, K. M. (2019). Impacts of Subtropical Highs on Summertime
870 Precipitation in North America. *Journal of Geophysical Research: Atmospheres*, 124(21),
871 11188-11204. <https://agupubs.onlinelibrary.wiley.com/doi/abs/10.1029/2019JD031282>
- 872 Schnell, J. L., Holmes, C. D., Jangam, A., & Prather, M. J. (2014). Skill in forecasting extreme
873 ozone pollution episodes with a global atmospheric chemistry model. *Atmos. Chem. Phys.*,
874 14(15), 7721-7739. <http://www.atmos-chem-phys.net/14/7721/2014/>
- 875 Schnell, J. L., & Prather, M. J. (2017). Co-occurrence of extremes in surface ozone, particulate
876 matter, and temperature over eastern North America. *Proceedings of the National Academy of*
877 *Sciences*, 201614453. <https://www.pnas.org/content/pnas/early/2017/02/21/1614453114.full.pdf>
- 878 Schnell, J. L., Prather, M. J., Josse, B., Naik, V., Horowitz, L. W., Cameron-Smith, P., et al.
879 (2015). Use of North American and European air quality networks to evaluate global chemistry–

- 880 climate modeling of surface ozone. *Atmos. Chem. Phys.*, *15*(18), 10581-10596.
881 <https://acp.copernicus.org/articles/15/10581/2015/>
- 882 Schnell, J. L., Prather, M. J., Josse, B., Naik, V., Horowitz, L. W., Zeng, G., et al. (2016). Effect
883 of climate change on surface ozone over North America, Europe, and East Asia. *Geophysical*
884 *Research Letters*, *43*(7), 3509-3518.
885 <https://agupubs.onlinelibrary.wiley.com/doi/abs/10.1002/2016GL068060>
- 886 Shaposhnikov, D., Revich, B., Bellander, T., Bedada, G. B., Bottai, M., Kharkova, T., et al.
887 (2014). Mortality related to air pollution with the moscow heat wave and wildfire of 2010.
888 *Epidemiology (Cambridge, Mass.)*, *25*(3), 359-364. <https://pubmed.ncbi.nlm.nih.gov/24598414>
- 889 Shen, L., Mickley, L. J., & Gilleland, E. (2016). Impact of increasing heat waves on U.S. ozone
890 episodes in the 2050s: Results from a multimodel analysis using extreme value theory.
891 *Geophysical Research Letters*, *43*(8), 4017-4025.
892 <https://agupubs.onlinelibrary.wiley.com/doi/abs/10.1002/2016GL068432>
- 893 Simon, H., Reff, A., Wells, B., Xing, J., & Frank, N. (2015). Ozone Trends Across the United
894 States over a Period of Decreasing NO_x and VOC Emissions. *Environmental Science &*
895 *Technology*, *49*(1), 186-195. <https://doi.org/10.1021/es504514z>
- 896 Skyllakou, K., Garcia Rivera, P., Dinkelacker, B., Karnezi, E., Kioutsioukis, I., Hernandez, C., et
897 al. (2021). Changes in PM_{2.5} concentrations and their sources in the US from 1990 to 2010.
898 *Atmos. Chem. Phys. Discuss.*, *2021*, 1-34. <https://acp.copernicus.org/preprints/acp-2021-495/>
- 899 Solomon, P. A., Crumpler, D., Flanagan, J. B., Jayanty, R. K. M., Rickman, E. E., & McDade, C.
900 E. (2014). U.S. National PM_{2.5} Chemical Speciation Monitoring Networks—CSN and
901 IMPROVE: Description of networks. *Journal of the Air & Waste Management Association*,
902 *64*(12), 1410-1438. <https://doi.org/10.1080/10962247.2014.956904>
- 903 Spracklen, D. V., Mickley, L. J., Logan, J. A., Hudman, R. C., Yevich, R., Flannigan, M. D., &
904 Westerling, A. L. (2009). Impacts of climate change from 2000 to 2050 on wildfire activity and
905 carbonaceous aerosol concentrations in the western United States. *J. Geophys. Res.*, *114*(D20),
906 D20301. <http://dx.doi.org/10.1029/2008JD010966>
- 907 Sun, W., Hess, P., Chen, G., & Tilmes, S. (2019). How waviness in the circulation changes
908 surface ozone: a viewpoint using local finite-amplitude wave activity. *Atmos. Chem. Phys.*,
909 *19*(20), 12917-12933. <https://acp.copernicus.org/articles/19/12917/2019/>
- 910 Sun, W., Hess, P., & Liu, C. (2017). The impact of meteorological persistence on the distribution
911 and extremes of ozone. *Geophysical Research Letters*, *44*(3), 1545-1553.
912 <https://agupubs.onlinelibrary.wiley.com/doi/abs/10.1002/2016GL071731>
- 913 Tai, A. P. K., L.J. Mickley, & Jacob, D. J. (2010). Correlations between fine particulate matter
914 (PM_{2.5}) and meteorological variables in the United States: Implications for the sensitivity of
915 PM_{2.5} to climate change. *Atmospheric Environment*, *44*(32), 3976-3984.
916 [http://www.sciencedirect.com/science/article/B6VH3-50GWNDS-](http://www.sciencedirect.com/science/article/B6VH3-50GWNDS-3/2/df35554565c3e1b79bac2a652ca96aa4)
917 [3/2/df35554565c3e1b79bac2a652ca96aa4](http://www.sciencedirect.com/science/article/B6VH3-50GWNDS-3/2/df35554565c3e1b79bac2a652ca96aa4)
- 918 Tai, A. P. K., Mickley, L. J., Jacob, D. J., Leibensperger, E. M., Zhang, L., Fisher, J. A., & Pye,
919 H. O. T. (2012). Meteorological modes of variability for fine particulate matter (PM_{2.5}) air
920 quality in the United States: implications for PM_{2.5} sensitivity to climate change. *Atmos. Chem.*
921 *Phys.*, *12*(6), 3131-3145. <http://www.atmos-chem-phys.net/12/3131/2012/>

- 922 <http://www.atmos-chem-phys.net/12/3131/2012/acp-12-3131-2012.pdf>
- 923 Tang, Y., Winkler, J., Zhong, S., Bian, X., Doubler, D., Yu, L., & Walters, C. (2017). Future
924 changes in the climatology of the Great Plains low-level jet derived from fine resolution multi-
925 model simulations. *Scientific Reports*, 7(1), 5029. <https://doi.org/10.1038/s41598-017-05135-0>
- 926 Tawfik, A. B., & Steiner, A. L. (2013). A proposed physical mechanism for ozone-meteorology
927 correlations using land-atmosphere coupling regimes. *Atmospheric Environment*, 72, 50-59.
928 <https://www.sciencedirect.com/science/article/pii/S1352231013001672>
- 929 Turnock, S. T., Allen, R. J., Andrews, M., Bauer, S. E., Emmons, L., Good, P., et al. (2020).
930 Historical and future changes in air pollutants from CMIP6 models. *Atmos. Chem. Phys.*
931 *Discuss.*, 2020, 1-40. <https://www.atmos-chem-phys-discuss.net/acp-2019-1211/>
- 932 Vukovich, F. M. (1995). Regional-scale boundary layer ozone variations in the eastern United
933 States and their association with meteorological variations. *Atmos. Environ.*, 29, 2259-2273.
- 934 Wang, J. X. L., & Angell, J. K. (1999). Air stagnation climatology for the United States (1948-
935 1998). *NOAA/Air Resources Laboratory ATLAS No. 1*.
- 936 Weaver, C. P., Cooter, E., Gilliam, R., Gilliland, A., Grambsch, A., Grano, D., et al. (2009). A
937 Preliminary Synthesis of Modeled Climate Change Impacts on U.S. Regional Ozone
938 Concentrations. *Bulletin of the American Meteorological Society*, 90(12), 1843-1863.
939 <http://journals.ametsoc.org/doi/abs/10.1175/2009BAMS2568.1>
- 940 Wilks, D. S. (1995). *Statistical Methods in the Atmospheric Sciences*. San Diego, California:
941 Academic.
- 942 Wu, S. L., Mickley, L. J., Leibensperger, E. M., Jacob, D. J., Rind, D., & Streets, D. G. (2008).
943 Effects of 2000-2050 global change on ozone air quality in the United States. *Journal of*
944 *Geophysical Research - Atmospheres*, 113(D6), D06302.
- 945 Wu, X., Xu, Y., Kumar, R., & Barth, M. (2019). Separating Emission and Meteorological
946 Drivers of Mid-21st-Century Air Quality Changes in India Based on Multiyear Global-
947 Regional Chemistry-Climate Simulations. *Journal of Geophysical Research: Atmospheres*,
948 124(23), 13420-13438. <https://agupubs.onlinelibrary.wiley.com/doi/abs/10.1029/2019JD030988>
- 949 Xu, Y., & Lamarque, J.-F. (2018). Isolating the Meteorological Impact of 21st Century GHG
950 Warming on the Removal and Atmospheric Loading of Anthropogenic Fine Particulate Matter
951 Pollution at Global Scale. *Earth's Future*, 6(3), 428-440.
952 <https://agupubs.onlinelibrary.wiley.com/doi/abs/10.1002/2017EF000684>
- 953 Xu, Y., Wu, X., Kumar, R., Barth, M., Diao, C., Gao, M., et al. (2020). Substantial Increase in
954 the Joint Occurrence and Human Exposure of Heatwave and High-PM Hazards Over South Asia
955 in the Mid-21st Century. *AGU Advances*, 1(2), e2019AV000103.
956 <https://agupubs.onlinelibrary.wiley.com/doi/abs/10.1029/2019AV000103>
- 957 Zhang, J., Gao, Y., Luo, K., Leung, L. R., Zhang, Y., Wang, K., & Fan, J. (2018). Impacts of
958 compound extreme weather events on ozone in the present and future. *Atmos. Chem. Phys.*,
959 18(13), 9861-9877. <https://acp.copernicus.org/articles/18/9861/2018/>
- 960 Zhang, Y., & Wang, Y. (2016). Climate-driven ground-level ozone extreme in the fall over the
961 Southeast United States. *Proceedings of the National Academy of Sciences*, 113(36), 10025-
962 10030. <https://www.pnas.org/content/pnas/113/36/10025.full.pdf>